Intensity of the Earth's magnetic field: evidence for a Mid-Paleozoic dipole low

Louise M. A. Hawkins[1]*, J. Michael Grappone[1], Courtney J. Sprain[1,2], Patipan Saengduean[1,*3], Edward J. Sage[1,*4], Sheikerra Thomas-Cunningham[1], Banusha Kugabalan[1,*5], Andrew J. Biggin[1]

[1]Geomagnetism Laboratory, Department of Earth, Ocean and Ecological Sciences, University of Liverpool, Liverpool L69 7ZE, United Kingdom

[2]Department of Geological Sciences, The University of Florida, 241 Williamson Hall, PO Box 112120, Gainesville, FL 32611, United States

[*3]Department of Geophysics, Colorado School of Mines, 1500 Illinois St., Golden, CO 80401, United States

[*4]CGG Mapping Solutions, Crockham Park, Edenbridge, Kent, TN8 6SR, United Kingdom

[*5]School of Physics & Astronomy, Kelvin Building, University of Glasgow, Glasgow, G12 8QQ, Scotland, United Kingdom

*Louise M. A. Hawkins, Geomagnetism Laboratory, Department of Earth, Ocean and Ecological Sciences, University of Liverpool, Liverpool L69 7ZE, United Kingdom, +447790893332

Email: louisemahawkins@gmail.com

Abstract

The Mesozoic Dipole Low (MDL) is a period, covering at least ~80 million years, of low dipole moment that ended at the start of the Cretaceous Normal Superchron. Recent studies of Devonian age Siberian localities identified similarly low field values a few tens of million years prior to the Permo-Carboniferous Reverse Superchron (PCRS). To constrain the length and timing of this potential new dipole low, this study presents new paleointensity estimates from Strathmore (~411-416 Ma) and Kinghorn (~332 Ma) lava flows, UK. Both localities have been studied for paleomagnetic poles (Q values of 6-7) and the sites were assessed for their suitability for paleointensity from paleodirections, rock magnetic analysis, and microscopy. Thermal- and microwave-IZZI protocol experiments were used to determine site mean paleointensity estimates of ~3-51 µT (6-98 ZAm^2) and 4-11 µT (9-27 ZAm^2) from the Strathmore and Kinghorn localities, respectively. These, and all the sites from 200-500 Ma from the (updated) PINT15 database, were assessed using the Qualitative Paleointensity criteria (Q_{PI}). The procurement of reliable (Q_{PI} ≥5), weak paleointensity estimates from this and other studies indicates a period of low dipole moment (median field strength of 17 ZAm^2) for ~80 Myrs, from 332-416 Ma. This "Mid-Paleozoic Dipole Low (MPDL)" bears a number of similarities to the MDL, including the substantial increase in field strength near the onset of the PCRS. The MPDL also adds support to inverse relationship between reversal frequency and field strength and a possible ~200-million-year cycle in paleomagnetic behavior relating to mantle convection.

Significance Statement

Variations in past geomagnetic field strength are important indicators of variation in deep-Earth processes over hundreds of millions of years. Most other geophysical methods only provide a snapshot of the Earth's recent interior and deep Earth materials are poorly represented in the geological record. New measurements from Scotland (Northern UK), in addition to the existing datasets, show the field was relatively weak (less than half the strength of the long-term average field) for tens of millions of years between 332-416 Ma. The similarities between this and a later period of low field strength provide further evidence for a ~200-million-year cycle linked to deep Earth processes.

Introduction

The evolution of the Earth's deep interior, although critical to our understanding of the planet's history, is poorly constrained. Reconstructions of convection patterns, such as the configuration and volume of subduction through time (1, 2) and the occurrence of mantle plumes (often inferred from the occurrence of Large Igneous Provinces) (3), as well as the stability of the Large Low-Shear Wave Velocity Provinces (4), are generally ill defined prior to ~300 Ma. This lack of constraint is primarily due to poor preservation of materials that formed deep within the Earth and because most geophysical techniques (i.e. seismic tomography, gravity inversion, etc.) can only constrain geologically recent, deep Earth processes. Comparatively, the paleomagnetic record, and paleointensity in particular, has the potential to serve as a key indicator of early deep Earth processes, such as the initiation of the geodynamo (5) and inner core nucleation (6, 7). During the Phanerozoic, superchrons (periods of tens of millions of years without magnetic polarity reversals) are suggested to be linked to changes in Earth's deep interior (8, 9). Three superchrons have been identified (10) and correspond with peaks in field strength (11). The superchrons alternate with suspected periods of frequently-reversing weak dipole moments. If confirmed, this pattern would suggest at the existence of a ~200-million-year (Myr) cycle in paleomagnetic behavior, likely resulting from deep Earth processes (8), which alternates between superchrons and these periods of low magnetic dipole moments, such as the Mesozoic Dipole Low (MDL). First proposed by Prevot et al. (12), the MDL is a period of low dipole moment suggested to have lasted for at least the ~80 Myrs preceding the Cretaceous Normal Superchron (CNS: 84-126 Ma). The MDL has since been confirmed by subsequent studies (13, 14), which have potentially placed its origin near the end of the Permo-Carboniferous (Kiaman) Reversed Superchron (PCRS; 267-315 Ma) (15). It has also been suggested that the MDL is actually confined to ~150-170 Ma, while the rest of the "MDL" is biased towards low field values due to rock magnetic effects (16). Recent research from Siberian sites (17, 18) found a similar, persistent low dipole strength magnetic field during the Devonian (359 – 419 Ma), lasting ~50 Myrs, ~35 Myrs prior to the start of the PCRS. However, it is still unclear if the behavior of the magnetic field during the Devonian and Early Carboniferous (~100 Myrs pre-PCRS) is comparable to that of the MDL, as there is very little available data, with only five studies from this age in the Paleointensity Database (PINT15) (19).

To quantify the length of this potential dipole low, two localities from the east coast of Scotland, UK, were selected from this time period to augment the previously published studies (Fig. 1). The first of these, lava flows from the Strathmore region (411-416 Ma) (20), were initially studied comprehensively by Sallomy and Piper (21), who found paleodirections consistent with this early Devonian age. A follow-up paleointensity study by Kono (22), based on a subset of these sites, gave a mean virtual dipole moment (VDM) of ~35 ZAm^2, which is substantially lower than the present-day field strength (~80 ZAm^2). However, developments in the field of paleointensity in the last 40 years mean that the reliability of this study is now uncertain, as it was done prior to the development of modern day paleointensity techniques and selection criteria. No checks for alteration or multi-domain behavior were included, and recent studies have shown that the perpendicular protocol that was used therein can give artificially low paleointensities (23). The original paleodirectional study has also since been superseded by Torsvik (24). This updated study argued that the high degree of scatter and the presence of sites with 'transitional' directions in the original study, several of which were used for paleointensity, was likely due to bias introduced by the demagnetization techniques used and local tectonic effects.

The second locality, lava flows from the beaches along Kinghorn and Burntisland, Scotland (332 ± 5.6) (25), has not been studied for paleointensity previously. A paleodirectional study carried out on these lavas by Torsvik (26) found primary directions that were used to determine an Early Carboniferous pole. The new experimental results are presented herein alongside a detailed meta-analysis of published datasets dated to 200–500 Ma using paleointensity quality criteria (Q_{PI}) (27). The outcome supports a new key feature of long-term geomagnetic behavior: the mid-Paleozoic dipole low (MPDL).

Materials and Methods

Detailed geological backgrounds of the Strathmore and Kinghorn localities, along with a description of the sampling techniques used, are provided in *Geological Background and Sampling (SI)* and the location of the sites sampled are shown in Fig. 1. The suitability of these sites for paleointensity analysis was first determined using paleodirectional and rock magnetic analysis. The majority of sites were initially stepwise thermally demagnetized (see *Methods: Paleodirections (SI)* for details) to determine if the samples carried a stable magnetic remanence. Selection criteria applied to the individual paleodirections obtained were an anchored, maximum angular deviation (MAD_{ANC} ≤10°) and the angle between the anchored and unanchored directions (α ≤10°). Additionally, site directions required some degree of clustering (k ≥15), before being compared with those from the previous studies (24, 26) to determine if the magnetization was of the correct age. Rock magnetic analysis was also performed on all sites, including hysteresis, isothermal remanent magnetization (IRM), back-field, and thermomagnetic (Curie) measurements (see *Methods: Rock Magnetism (SI)* for details). These measurements, in conjunction with scanning electron microscopy (SEM) analysis, were used to determine if the remanence carriers were consistent with the sites carrying a primary Thermal Remanent Magnetization (TRM). Sites that passed all the criteria were then used for paleointensity analysis. Both microwave and thermal Thellier-type paleointensity experiments were performed using the IZZI protocol (28) with partial TRM (pTRM) checks (29). Full details of the experimental procedure used, including selection criteria applied, is provided in *Methods: Paleointensity (SI)*.

Results

Strathmore paleointensity. A detailed outline of the results of the paleodirectional and rock magnetism analysis carried out on this locality is described under *Strathmore Results (SI)*. Based on these results, of the eleven Strathmore sites that gave acceptable paleodirections, six were determined to be suitable for paleointensity experimentation. The five sites that produced thermomagnetic curves consistent with (titano-)maghemite (CB2-CB4, TH1 and SN3) were excluded from further analysis because (titano-)maghemite is unlikely to be the original (primary) mineralogy of these lavas (see *Strathmore Results; Rock Magnetism (SI);* Fig. S3a). Comparatively, the sites measured for paleointensity were deemed to likely retain a primary TRM. Sites CB1 and SN1 produced thermomagnetic curves that indicated the presence of two magnetic minerals, magnetite and hematite (Fig. S3b). The unblocking temperature range of the ChRM supports that the primary remanence is carried by both minerals (see Fig. S1bi and *Strathmore Results; Rock Magnetism* for details*)*. The remaining sites (WB2-WB5) produced thermomagnetic curves consistent with magnetite (Fig. S3d) and gave representative SEM microscopy that showed no evidence of low temperature oxidation (Fig. S3g). Site WB2 was combined with the hematite-bearing (Fig. S3c) baked sediment (WB1) into a single paleointensity site (WB1/2) because the similar characteristic remanent magnetisation (ChRM) directions for the two sites (*see Strathmore Results; Paleodirections (SI) for details*) suggests that

WB1 was completely remagnetized by the overlying lava (WB2), which means they would have acquired their TRM in the same field.

From the Strathmore locality, 35 out of 82 paleointensity measurements passed selection criteria (given in Table S1; pass rate of 43%) across the six sites. All but one site gave low site-mean paleointensity estimates (3.1-19.7 μT), corresponding to VDMs between 5.6 and 46.2 ZAm^2 (Table 1), while site CB1 gave a singularly high site mean estimate of 50.9 μT (98.0 ZAm^2). The majority of accepted Strathmore estimates are from thermal experiments because the microwave demagnetization mechanism was largely unsuitable for hematite bearing sites (CB1, SN1, WB1). The other estimates were split approximately evenly between the two techniques. The pass rate for microwave experiments was 48% vs. 36% for thermal results for the sites that used both methods. Characteristic Arai plots (Fig. 2) show the range of behavior exhibited from the six sites and the different techniques used. The hematite-bearing sites (Fig. 2a-b) showed minimal demagnetization at temperatures below 300°C and linear Arai plots across the temperature ranges for magnetite or both magnetite and hematite. From Wormit Bay, sites WB2-WB3 (Fig. 2c-d) behave similarly, as do WB4-WB5 (Fig. 2e-f), likely because of the similarities in grain size, based on the hysteresis properties of the sites (Fig S3i). Sites WB2-WB3 lie close to the MD range but produce near-linear orthogonal vector and Arai plots, whereas sites WB4-WB5 exhibit some zig-zagging of the corresponding orthogonal plots and the main occurrence of prominently two-sloped Arai plots; however, as seen in the orthogonal plots from the corresponding thermal demagnetization experiments (Fig. S1di), the samples display more than one directional component, and the temperature range of the ChRM corresponds to the selected component from the thermal paleointensity experiments. Accepted measurements are considered unaffected by anisotropy, based on measurement gamma values (γ), and non-linear TRM effects, as both the ancient and applied fields used are relatively low (≤60 μT). The Wormit Bay sites are also unlikely to have been affected by cooling rate based on the samples' grain size distribution (non-single domain (SD) grains (30); Fig S2i) and any variation between results from techniques with different cooling rates (thermal vs. microwave) or mineralogy with different grain size distributions (magnetite vs. hematite) being inconsistent with the expected effects from cooling rate differences (see *Paleointensity Reliability Assessment; Strathmore Q_{PI} scoring*, the ACN criterion, for further details).

Kinghorn paleointensity. A detailed outline of the results of the paleodirectional and rock magnetism analysis carried out on this locality is described under *Kinghorn Results (SI).* All the Kinghorn sites that passed the paleodirectional selection criteria (six out of nine sites) were deemed suitable for paleointensity, along with two additional sites (KHA-KHB; Fig. S2b), for a total of eight paleointensity sites. Some sites had curves that were consistent with relatively Ti-rich titanomagnetite. (KH1 and KHA-KHB; Fig. S3f), while the rest (KH2, KH4 and KH7-KH10; KH8/9 is a single site) were consistent with magnetite or low-Ti titanomagnetite (Fig. S3e). Representative SEM microscopy showed primary igneous textures (i.e. coarse exsolution structures) and no evidence of low temperature oxidation (Fig. S3h), which is consistent with the sites carrying a primary TRM.

Of the Kinghorn locality samples, 53 out of 143 measurements passed selection criteria (given in Table S2; pass rate of 37%). All sites produced very low site mean estimates (3.7-10.9 µT; Table 1), corresponding to exceptionally low VDM estimates (9.6-27.0 ZAm^2). The majority of the accepted measurements were made using the microwave system, as it had a much higher success rate (54% success rate vs. the 9% success rate for thermal experiments). This may be because the relatively Ti-rich titanomagnetite is prone to altering more in the thermal than the microwave experiments due to reduced bulk heating of the samples in the latter (31). The appearance of the Arai plots varies, with some sites producing near linear plots with minimal overprints (Fig. 2a, f), whereas others exhibit varying degrees of two-slope behavior (Fig 2b-e). Like sites WB4-WB5, the two-slope Arai plots all show a corresponding change in direction, which is also indicated in the thermal demagnetization orthogonal plots (Fig. S1ei-fi). These plots suggest that the steep, low-temperature slope is likely an overprint rather than due to non-ideal behavior. This interpretation is also supported by a lack of zig-zagging when using IZZI protocol and the low degrees of curvature (which was evaluated using curvature, $|k'|$). There is no clear correlation between the appearance of the Arai plots and either the titanium content of the titanomagnetite or the apparent grain size (Fig. S3j). Accepted measurements are considered unaffected by cooling rate, due to the samples' non-SD grain size (Fig S2j) and the lavas being "fast-cooled" (27), and non-linear TRM effects (for the same reason as the Strathmore sites). Anisotropy checks on the Kinghorn samples, performed due to relatively high γ values, show that some of the Kinghorn sites are slightly anisotropic, but the anisotropic corrections required (which vary depend on the applied field direction) are negligible and average out to give nearly identical results to the uncorrected site means (see *Paleointensity Reliability Assessment; Kinghorn Q_{PI} scoring,* the ACN criterion, for further details and quantification).

Discussion

Reliability of 200-500 Ma sites. To further assess the reliability of these new site-mean paleointensity estimates, and to provide a framework for comparing them to others from the Paleozoic (~252-541 Ma), all sites were evaluated using Q_{PI} criteria. Biggin and Paterson (32) proposed these nine criteria to acknowledge and mitigate the potential biases that affect the interpretation of paleointensity data and are applied in a similar way to Q criteria for paleomagnetic poles (33). Sites that have published information addressing a criterion pass (score a 1), and, if not, they fail (score a 0). The Q_{PI} score for the site is the sum of the individual criterion scores. Detailed descriptions of these nine Q_{PI} criteria and how they have been assessed for this study are included in *Paleointensity Reliability Assessment; Q_{PI} criteria (SI)* and explanations for how the Kinghorn and Strathmore sites were scored is provided in *Paleointensity Reliability Assessment; Strathmore scoring* and *Kinghorn scoring (SI)* respectively. A summary of the individual criteria scores for each site is provided in Table 1 and in Dataset S3. The new Strathmore sites in this study received Q_{PI} scores ranging from 5 to 8 (median: 6.5, mean: 6.3), out of a possible 9. The new Kinghorn sites similarly received Q_{PI} scores ranging from 6 to 8 (with a slightly higher median of 7 and mean of 6.8). STAT and LITH are the Q_{PI} criteria that the majority of sites failed. The failure to meet STAT is largely because the sites gave low paleointensity estimates, which are less likely to pass STAT due to its definition (see *Paleointensity Reliability Assessment; Strathmore scoring for details (SI))*, and LITH because only one site had a suitable contact lithology that could be sampled. MD and TRM failing for some of the Strathmore sites is why its Q_{PI} scores are slightly lower than those of the Kinghorn sites. However, the sites are not considered unreliable as their failure to pass these criteria need not require that they have been remagnetized and/or affected by MD behavior. We note that our results are also very similar to those obtained from Siberian rocks of a similar age (7-39 ZAm^2 with a single outlier site of 98 ZAm^2) (17).

Integration of these new estimates with the existing Paleozoic dataset first requires determination of what published data are sufficiently robust for meta-analysis. All the data in the PINT15 database (19) from 200-500 Ma were checked against their corresponding study to fix any errors. Ages were recalculated where possible (e.g. stratigraphic ages were revised to be consistent with the most recent timescale (ICS2020/v1), isotopic ages were replaced where superseding ages are known, etc.). The biggest reassessment of site ages comes from the apparently Middle-Late Carboniferous from Uzbekistan (34, 35).The relative ages between sites and the single inclination sign across multiple sections, with 13-40 sites per section, indicate that these sites could only come from the part of the Carboniferous during the PCRS (i.e. Moscovian-Gzhelian; 298.9-315.2 Ma). Sites from 5 studies published since the last PINT15 update were also added (references listed in Dataset S4). Q_{PI} criteria were applied to all the sites, based on the published information from the corresponding studies. This time period covers both the PCRS and the surrounding time periods, which allows paleomagnetic field strengths during the superchron to be compared with those from a reversing field. This time period also complements two other Q_{PI} studies that assessed the PINT15 database for 500-3500 Ma (6) and 65-200 Ma (16).

The revised PINT15 data for 200-500 Ma, including Q_{PI} scoring, is included in Dataset S3. A workflow for the scores provided is outlined in Dataset S4, and the age distribution, coverage, and reliability of the revised 200-500 Ma PINT15 data is illustrated in Fig. 4. Given that most studies from this time period were published before Q_{PI} criteria existed, their Q_{PI} scores tend to be lower because there is insufficient information published to confirm that a potential issue has been addressed, rather than it being clear that that issue has affected the estimates. Only sites with Q_{PI} scores of 0 will be excluded entirely; these either have no published information to support the reliability of the site means or they have been confirmed to be unreliable. All the highest scoring sites (Q_{PI} ≥5) are found in the time periods immediately before (16 sites) and after (26 sites) the PCRS, which comprises the data from this study along with recently published studies (17, 18). While there are numerous sites with PCRS ages, 144 of the 195 sites (74%) covering this period come from just four studies: (34, 36–38). The Q_{PI} scores for these are low because these publications use outdated paleointensity methods (i.e. calculating the ratio of total NRM/total TRM) (39) and include very little supporting information.

Paleozoic Field Variation. Based on the pattern of field strength variation from these new site means and the existing PINT15 dataset, weighted by Q_{PI} score (Fig.4), a relatively long period of low dipole moment presents itself in the period preceding the PCRS, followed by a substantial increase in field strength during the superchron relative to periods of reversing field. To evaluate whether this variation is similar to that observed during the Mesozoic, an analysis was performed, following the methodology of previous studies (6, 16), by comparing the field strength distribution of different periods, filtered by Q_{PI} scoring. The combined dataset was grouped into 3 bins using the superchron as an anchor: PRE (315-416 Ma), PCRS (267-315 Ma), and POST (200-267 Ma). Kulakov et al. (16) was able to identify periods of distinct dipole moment during the MDL based on reversal frequency. However, the reversal record prior to the PCRS is too sparse to apply the same technique (Fig. 4), so the PRE bin was not divided further. Its maximum age bound was set to 416 Ma to avoid the Ordovician Reversed Superchron (ORS; 461-480 Ma) (40) and because there are no estimates with $Q_{PI} \geq 1$ between 416-461 Ma. There is no analysis of the ORS, or the period before it, as between 461-500 Ma there are only 3 available estimates. The age distribution of the POST bin is also substantially skewed (skewness = -6.14 at $Q_{PI} \geq 3$; see Table S2) as there are only 13 site-mean results between 200-250 Ma and an abundance of data around ~250 Ma. This peak in the data is almost entirely the result of a large number of studies from the Siberian Traps (see Anwar et al. (15) for details); however, the paucity of data between 200-250 Ma means it cannot be connected to the Early bin from Kulakov et al. (16) and should be considered independent of it.

Q_{PI} filtering was applied based on the total Q_{PI} score for the site, up to a $Q_{PI} \geq 5$ (because the PCRS bin does not include any sites that have a total score greater than five). Fig. 5a-e illustrates the distribution of site VDMs in these bins for different Q_{PI} minima, while details of the data included in these bins are included in Table S2. However, not all the Q_{PI} criteria are considered to be of equal weight. As discussed in Kulakov et al. (16), AGE, STAT, TRM, MD and ALT are considered the priority criteria; however, it is not possible to make all these criteria mandatory and still have sufficiently large datasets for statistical analysis. AGE and ALT are considered essential criteria to retain (16), but the way the TRM criterion is judged (see *Paleointensity Reliability Assessment; Q_{PI} criteria (SI)*) means that a site can carry a TRM but not successfully meet the criterion. Too few PCRS sites pass TRM (11 sites) for further analysis to be statistically meaningful (especially when requiring AGE and ALT to pass as well). The inverse problem exists for the STAT criterion: very few sites pass the criterion for the PRE (18 sites) and POST (16 sites) bins, probably because of the weak site mean value, which is discussed in *Paleointensity Reliability Assessment; Kinghorn Scoring (SI).* However, requiring the inclusion of the MD criterion still retained a statistically rigorous number of sites across all three age bins (171 sites passed for AGE, ALT and MD). The inclusion of the MD criterion is also particularly important because MD effects on paleointensity experiments have been cited as a primary cause for the apparent long-lasting weak strength of the paleomagnetic field, compared to the present day field value (41). The distribution of VDMs that pass all these criteria (AGE+ALT+MD) is shown in Fig. 5f, and details of the data included in these bins are included in Table S2. Finally, to check that the bin statistics are not being biased by oversampling of the field at certain time periods (i.e. 250 Ma), the subsets of sites with total Q_{PI} scores ≥1 and ≥3, were binned in 10 Ma and 5 Ma intervals before averaging (details in Table S2).

A series of Kolomogorv-Smirnov (K-S) tests were run to compare the bins pair-wise (Table S2). The tests reject the null hypothesis that the datasets come from the same distribution at the 1% significance level up to Q_{PI} ≥5 (the PCRS and POST bins have too few data to be significant if a higher Q_{PI} cut-off is applied; see Table S2). All three time periods, therefore, have distinct VDM distributions. Fig. 5(a-f) indicates that the dipole moment during the PCRS is substantially higher than the surrounding time periods, regardless of Q_{PI} filtering, although its average strength is unclear. The median values for the PCRS range from 39–94 ZAm^2 depending on the Q_{PI} filters and binning used. Although the median CNS values (48-59 ZAm^2), based on similar analysis (16), fit within this range, the large range in average field strength during the PCRS points to issues with the current PCRS dataset. The difference emerges from the greater number of low estimates recorded for the CNS than the PCRS. The higher median values are generally from subsets with lower levels of reliability (low Q_{PI} scores/number of bins) because the four studies that make up the bulk of the PCRS are older studies that give generally high field values and have Q_{PI} scores ≤3. There are a greater number of, and more recent, studies available for the CNS, so the median values for it are more likely to represent reliable estimates of field strength during a superchron. Thus, while the difference in average field strength between the PCRS and the rest of the Paleozoic is likely to remain, further studies are needed to evaluate the average strength of the field during the PCRS and if the potential differences between the average field strength during the two superchrons is valid or due to data bias.

Both the PRE and POST bins gave consistently low values across all Q_{PI} filters (Fig. 5), including AGE + ALT + MD, suggesting that MD behavior is not responsible for the appearance of these periods of low field strength. Comparatively, the AGE + ALT + MD filter provided one of the lowest median values for the PCRS (48 ZAm^2) suggesting MD behavior could instead be biasing the PCRS values high (if taken from the lower temperature slope). The aging of TRM has also been considered as a potential cause of long-term field strength underestimation. While this process is less well understood than MD effects, experiments have shown that specimens affected by aging tend to show more pronounced MD-like behavior (42) so they should also be excluded by the MD criterion. Dividing the POST bin into 5 and 10 Ma intervals gives marginally higher field values. This result suggests that the low average field strength of the POST bin and, potentially, the distinct VDM distribution from the PRE bin (despite their similar median values), could be due to under-sampling of the average field behavior during this time bracket. As demonstrated by the highly skewed age of the bins and the low N values for 5 and 10 Ma sub-bins, almost all the sites from this time period were emplaced over ~800,000 years (the Siberian Trap sites) (43). The low N values mean that, while they may still be underestimating the long-term strength of the field, they are starting to approach the strength of the field following another superchron, the CNS (Late period; 36 ZAm^2 at Q_{PI} ≥3) (16).

The strength of the field prior to the PCRS is the most reliable period herein due to the consistency between the median values for the PRE bin, regardless of filtering and age binning. The new paleointensity data presented in this study are also in close agreement with previous studies, with median field estimates for the PRE bin ranging from 12.2-18.9 ZAm^2, based on the same filtering of Q_{PI} scores as used in Table S2. This range of median values for the PRE bin remains the same if sites from the Kinghorn locality or the Strathmore locality, or both, are excluded. The consistency between these new estimates and the legacy weak-field data, despite differences in reliability between the new sites and those from the older studies, is encouraging because it indicates the field strength during this time period is not being underestimated. At ~17 ZAm^2 (Q_{PI} ≥3), the PRE bin is considerably lower than the average for the Phanerozoic, which is estimated to be 42 ZAm^2 (13) to 50 ZAm^2 (6) and is probably the typical strength of the field outside of the Bruhnes (44); i.e., the period since the last geomagnetic field reversal (the last ~770 ka). The PRE bin values are closest in strength to the Jurassic Hyperactivity period (JHAP; 155-171 Ma; 26 ZAm^2 for all data points, 35 ZAm^2 at Q_{PI} ≥3 (45), which had an average reversal frequency of ~11 reversals/Myr. In comparison, the other periods of reversing field during the Mesozoic (Early, Mid, Late) had median field strengths of 36-48 ZAm^2, with reversal frequencies of 1-3 reversals/Myr. The low average field strength may be partly due to recent studies (with higher Q_{PI} scores) tending to sample periods of very high reversal frequency, like the JHAP. This tendency is difficult to constrain because the magnetostratigraphic records before the PCRS are generally too sparse to provide a reliable record of reversal frequency. A recent magnetostratigraphic study from the Canning Basin (46) suggests reversal frequencies of a minimum of 2-5 reversals/Myr around the same time that the Viluy sites cooled (~360 Ma) (18). In addition, an evaluation of reversal frequency ~8-14 Myrs before the PCRS (47) suggests reversal frequencies of ~12 reversals/Myr, very similar to the high JHAP values, occurring ~5 Myr after the Kinghorn lavas (this study) erupted. These studies produced notably weak site mean values in the range of 4–27 ZAm^2. A greater non-dipole component to the field, relative to the present day, is also indicated for some of the Siberian sites, such as the Minusa (17) and the aforementioned Viluy Traps (18), although the new sites herein provide no indication of a greater non-dipole component, despite comparable timing and field strength estimates.

A Mid-Paleozoic Dipole Low and its implications for deep mantle variation. Despite some potential biases of the dataset, as discussed in the previous sections, the evaluation of the period of low dipole moment leading up to the PCRS provided by this study suggests it is a significant and distinct feature of the Paleozoic paleomagnetic record (see K-S tests in Table S2).

The proposed term for this feature, the mid-Paleozoic dipole low (MPDL), is based on its similarities to the MDL. These similarities include the weak field (discussed in previous section) and the ~80 Myr duration, from ~416-332 Ma. In both cases, however, gaps in the record make it difficult to confirm if the period of low dipole moment extends back further in time (18). The average field strength has been shown to vary throughout the MDL (16), and there is also evidence for a difference (see Fig. 4) between the relatively strong early part of the MPDL in the interval 390-416 Ma (median of 36 ZAm^2), based on the Minusa (17) and Strathmore (this study) sites, and the rest of the MPDL (317-390 Ma; median of 14 ZAm^2). Unlike the MDL, the low field strength is difficult to relate directly to reversal frequency due to the paucity of magnetostratigraphic records at this time. Finally, there is a clear increase in field strength around the onset of the PCRS, estimated to be 3-4 times the strength of the pre-PCRS field if the average for the PCRS is reliable. We point out, however, that a gap in the dataset exists from ~20 Myrs prior to the PCRS to an unknown point in the superchron (assumed to be within the Carboniferous part of the PCRS; 299-315 Ma). The large age uncertainties associated with the early PCRS sites prevent a clear determination of this transition.

The newly assessed paleointensity record provided in this study gives an improved indication of patterns in Phanerozoic paleomagnetic field behavior across 10–100 Myr timescales (8) back to ~415 Ma. The similarities observed herein between the MPDL and the MDL prior to their respective superchrons provide more evidence for the proposed inverse relationship between field strength and reversal frequency. There are insufficient site-mean paleointensity estimates prior to (3 site means) and during (0 site means) the ORS to test this theory further back in time. There have been several mechanisms proposed for this variation in field behavior relating to mantle plumes (9, 48), subduction (2) and True Polar Wander (8). The extension of our reliable Phanerozoic paleointensity record will assist future studies in linking these processes to paleomagnetic evolution.

Acknowledgments

We would like to thank Elliot Hurst, Neil Suttie and Thomas Beckwith, who assisted in sample collection. LMH, CJS and AJB acknowledge funding NERC standard grant NE/P00170X/1. LMH further acknowledges funding from NERC Studentship 1511981. JMG acknowledges support from the NERC EAO Doctoral Training Programme (grant NE/L002469/1; studentship 1793213) and the Duncan Norman Research Scholarship. Both AJB and JMG further acknowledge funding from The Leverhulme Trust (RLA-2016-080).

References

1. D. G. van der Meer, D. J. J. van Hinsbergen, W. Spakman, Atlas of the underworld: Slab remnants in the mantle, their sinking history, and a new outlook on lower mantle viscosity. *Tectonophysics* **723**, 309–448 (2018).
2. M. W. Hounslow, M. Domeier, A. J. Biggin, Subduction flux modulates the geomagnetic polarity reversal rate. *Tectonophysics* **742**–**743**, 34–49 (2018).
3. R. E. Ernst, K. L. Buchan, “Large mafic magmatic events through time and links to mantle-plume heads” in *Mantle Plumes: Their Identification through Time*, R. E. Ernst, K. L. Buchan, Eds. (Geological Society of America, 2001), pp. 483–575.
4. T. H. Torsvik, K. Burke, B. Steinberger, S. J. Webb, L. D. Ashwal, Diamonds sampled by plumes from the core-mantle boundary. *Nature* **466**, 352–355 (2010).
5. J. A. Tarduno, R. D. Cottrell, W. J. Davis, F. Nimmo, R. K. Bono, A Hadean to Paleoarchean geodynamo recorded by single zircon crystals. *Science (80-.).* **349**, 521–524 (2015).
6. A. J. Biggin, *et al.*, Palaeomagnetic field intensity variations suggest Mesoproterozoic inner-core nucleation. *Nature* **526**, 245–248 (2015).
7. R. K. Bono, J. A. Tarduno, F. Nimmo, R. D. Cottrell, Young inner core inferred from Ediacaran ultra-low geomagnetic field intensity. *Nat. Geosci.* **12**, 143–147 (2019).
8. A. J. Biggin, *et al.*, Possible links between long-term geomagnetic variations and whole-mantle convection processes. *Nat. Geosci.* **5**, 526–533 (2012).
9. P. Olson, H. Amit, Mantle superplumes induce geomagnetic superchrons. *Front. Earth Sci.* **3**, 1–11 (2015).
10. V. Pavlov, Y. Gallet, A third superchron during the Early Paleozoic. *Episodes* **28**, 78–84 (2005).
11. L. Tauxe, H. Staudigel, Strength of the geomagnetic field in the Cretaceous Normal Superchron: New data from submarine basaltic glass of the Troodos Ophiolite.

Geochemistry, Geophys. Geosystems **5** (2004).

12. M. Prévot, M. E.-M. Derder, M. McWilliams, J. Thompson, Intensity of the Earth's magnetic field: Evidence for a Mesozoic dipole low. *Earth Planet. Sci. Lett.* **97**, 129–139 (1990).
13. L. Tauxe, J. S. Gee, M. B. Steiner, H. Staudigel, Paleointensity results from the Jurassic: New constraints from submarine basaltic glasses of ODP Site 801C. *Geochemistry, Geophys. Geosystems* **14** (2013).
14. D. N. Thomas, A. J. Biggin, Does the mesozoic dipole low really exist? *Eos Trans. AGU* **84**, 97–104 (2003).
15. T. Anwar, L. Hawkins, V. A. Kravchinsky, A. J. Biggin, V. E. Pavlov, Microwave paleointensities indicate a low paleomagnetic dipole moment at the Permo-Triassic boundary. *Phys. Earth Planet. Inter.* **260**, 62–73 (2016).
16. E. V Kulakov, *et al.*, Analysis of an updated paleointensity database (QPI-PINT) for 65-200 Ma: Implications for the long-term history of dipole moment through the Mesozoic. *J. Geophys. Res. Solid Earth* **124**, 9999–10022 (2019).
17. V. V. Shcherbakova, *et al.*, Was the Devonian geomagnetic field dipolar or multipolar? Palaeointensity studies of Devonian igneous rocks from the Minusa Basin (Siberia) and the Kola Peninsula dykes, Russia. *Geophys. J. Int.* **209**, 1265–1286 (2017).
18. L. M. A. Hawkins, *et al.*, An exceptionally weak Devonian geomagnetic field recorded by the Viluy Traps, Siberia. *Earth Planet. Sci. Lett.* **506**, 134–145 (2019).
19. A. J. Biggin, G. H. M. A. Strik, C. G. Langereis, The intensity of the geomagnetic field in the late-Archaean: New measurements and an analysis of the updated IAGA palaeointensity database. *Earth, Planets Sp.* **61**, 9–22 (2009).
20. M. F. Thirlwall, Geochronology of Late Caledonian magmatism in northern Britain. *J. Geol. Soc. London.* **145**, 951–967 (1988).
21. J. T. Sallomy, J. D. A. Piper, Palaeomagnetic Studies in the British Caledonides - IV Lower Devonian Lavas of the Strathmore Region. *Geophys. Journal, R. Astron. Soc.* **34**, 47–68 (1973).
22. M. Kono, Palaeomagnetism and palaeointensity studies of Scottish Devonian volcanic rocks. *Geophys. J. Int.* **56**, 385–396 (1979).

23. J. M. Grappone, A. J. Biggin, M. J. Hill, Solving the mystery of the 1960 Hawaiian lava flow: implications for estimating Earth's magnetic field. *Geophys. J. Int.* **218**, 1796–1806 (2019).
24. T. H. Torsvik, Magnetic properties of the Lower Old Red Sandstone lavas in the Midland Valley, Scotland; palaeomagnetic and tectonic considerations. *Phys. Earth Planet. Inter.* **39**, 194–207 (1985).
25. S. Brindley, E. Spinner, Palynological assemblages from Lower Carboniferous deposits, Burntisland district, Fife, Scotland. *Proc. Yorksh. Geol. Soc.* **47**, 215–231 (1989).
26. T. H. Torsvik, O. Lyse, G. Atterás, B. J. Bluck, Palaeozoic palaeomagnetic results from Scotland and their bearing on the British apparent polar wander path. *Phys. Earth Planet. Inter.* **55**, 93–105 (1989).
27. A. J. Biggin, G. A. Paterson, A new set of qualitative reliability criteria to aid inferences on palaeomagnetic dipole moment variations through geological time. *Front. Earth Sci.* **2**, 1–9 (2014).
28. Y. Yu, L. Tauxe, Testing the IZZI protocol of geomagnetic field intensity determination. *Geochemistry, Geophys. Geosystems* **6** (2005).
29. R. S. Coe, S. Grommé, E. A. Mankinen, Geomagnetic paleointensities from radiocarbon-dated lava flows on Hawaii and the question of the Pacific nondipole low. *J. Geophys. Res.* **83**, 1740–1756 (1978).
30. A. J. Biggin, S. Badejo, A. R. Muxworthy, M. J. Dekkers, The effect of cooling rate on the intensity of thermoremanent magnetization (TRM) acquired by assemblages of pseudo-single domain, multidomain and interacting single-domain grains. *Geophys. J. Int.* **193**, 1239–1249 (2013).
31. N. Suttie, J. Shaw, M. J. Hill, Direct demonstration of microwave demagnetization of a whole rock sample with minimal heating. *Earth Planet. Sci. Lett.* **292**, 357–362 (2010).
32. G. A. Paterson, L. Tauxe, A. J. Biggin, R. Shaar, L. C. Jonestrask, On improving the selection of Thellier-type paleointensity data. *Geochemistry, Geophys. Geosystems* **15**, 1180–1192 (2014).
33. R. Van der Voo, The reliability of paleomagnetic data. *Tectonophysics* **184**, 1–9 (1990).
34. G. M. Solodovnikov, Paleostrength of thegeomagnetic field in Middle-Late Carboniferous.

Izv. - Phys. Solid Earth **28**, 327–331 (1992).

35. G. M. Solodovnikov, Geomagnetic intensity in the Middle Carboniferous of Uzbekistan. *Izv. - Russ. Acad. Sci. Phys. Solid Earth* **28**, 511–515 (1993).
36. W. E. Senanayake, M. W. McElhinny, A palaeointensity method for use with highly oxidised basalts, and application to some Permian volcanics. *J. Geophys.* **52**, 85–96 (1983).
37. A. S. Bolshakov, G. M. Solodovnikov, Y. K. Vinogradov, Paleointensity of the Geomagnetic Field in the Early Permian. *Izv. - Phys. Solid Earth*, 70–78 (1989).
38. G. M. Solodovnikov, Paleointesnity of the geomagnetic field in the Lower Permian. *Izv. - Phys. Solid Earth* **28**, 718–722 (1992).
39. J. G. Koenigsberger, Natural residual magnetism of eruptive rocks. *Terr. Magn. Atmos. Electr.* **43**, 299 (1938).
40. J. G. Ogg, G. Ogg, F. M. Gradstein, *A concise geologic time scale 2016. [electronic book]* (2016).
41. A. V. Smirnov, E. V. Kulakov, M. S. Foucher, K. E. Bristol, Intrinsic paleointensity bias and the long-term history of the geodynamo. *Sci. Adv.* **3** (2017).
42. R. Shaar, L. Tauxe, Instability of thermoremanence and the problem of estimating the ancient geomagnetic field strength from non-single-domain recorders. *Proc. Natl. Acad. Sci. U. S. A.* **112**, 11187–11192 (2015).
43. S. D. Burgess, S. A. Bowring, High-precision geochronology confirms voluminous magmatism before, during, and after Earth’s most severe extinction. *Sci. Adv.* **1** (2015).
44. G. Cromwell, L. Tauxe, S. A. Halldõrsson, New paleointensity results from rapidly cooled Icelandic lavas: Implications for Arctic geomagnetic field strength. *J. Geophys. Res. Solid Earth* **120**, 2913–2934 (2015).
45. M. Tominaga, W. W. Sager, M. A. Tivey, S.-M. Lee, Deep-tow magnetic anomaly study of the Pacific Jurassic Quiet Zone and implications for the geomagnetic polarity reversal timescale and geomagnetic field behavior. *J. Geophys. Res. Solid Earth* **113**, B07110 (2008).
46. J. Hansma, *et al.*, Late Devonian carbonate magnetostratigraphy from the Oscar and Horse Spring Ranges, Lennard Shelf, Canning Basin, Western Australia. *Earth Planet. Sci.*

Lett. **409**, 232–242 (2015).

47. M. W. Hounslow, Geomagnetic reversal rates following Palaeozoic superchrons have a fast restart mechanism. *Nat. Commun.* **7** (2016).
48. H. Amit, P. Olson, Lower mantle superplume growth excites geomagnetic reversals. *Earth Planet. Sci. Lett.* **414**, 68–76 (2015).
49. G. A. Paterson, A simple test for the presence of multidomain behavior during paleointensity experiments. *J. Geophys. Res. Solid Earth* **116** (2011).
50. E. Thébault, *et al.*, International Geomagnetic Reference Field: the 12th generation. *Earth, Planets Sp.* **67**, 79 (2015).

Figures and Tables

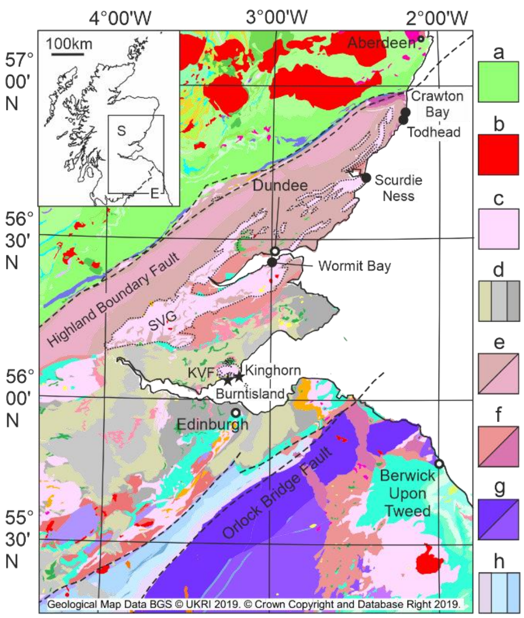

Figure 1. Geological map showing the Strathmore (black circles) and Kinghorn (black stars) localities sampled for paleodirection and paleointensity sites in this study. The geological units come from the is the 1:50000 solid geology map from the British Geological Survey (BGS) ©UKRI 2019, accessed via Edina Digimap, and generalized descriptions are listed in the legend on the right. Key cities are highlighted as white circles and key faults as dashed lines. The Strathmore Group Volcanic (SGV) units and the Kinghorn Volcanic Formation (KVF) are highlighted with dotted outlines. The location of the geological map in outlined in the inset map in the top left corner of the Northern UK. The metamorphic and igneous geological units are a) Neoproterozoic metamorphics, b) Silurian-Early Devonian felsic intrusions, c) Silurian–Devonian mafic extrusives. The remaining units are clastic sedimentary rocks from d) Visean to Westphalian, e) Arbuthnott-Garvock/Strathmore Groups, f) other Devonian, g) Llandovery-Wenlock and h) Caradoc to Ashgill.

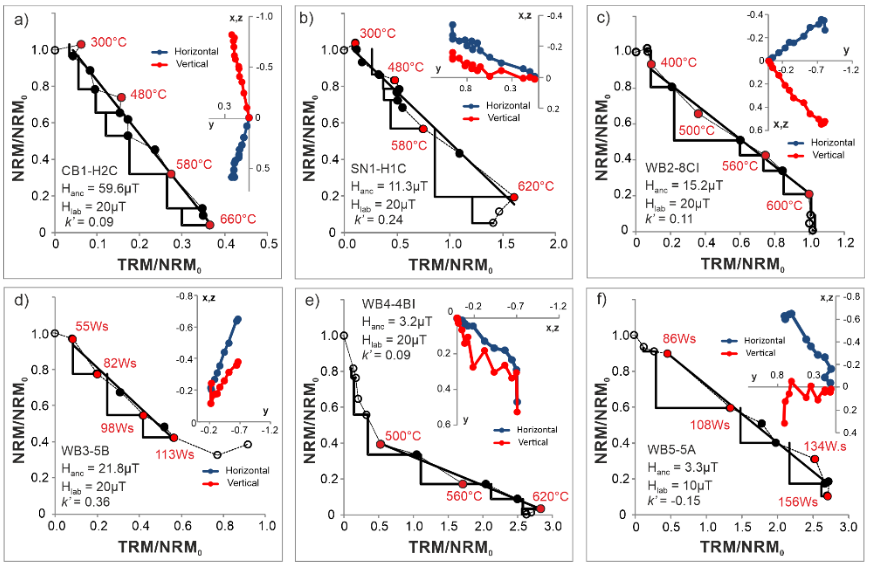

Figure 2. Representative Arai plots from the six Strathmore sites a) CB1, b) SN1, c) WB(1/)2, d) WB3, e) WB4 and f) WB5, illustrating the different Arai plot behaviors observed. All the measurements were done using microwave and thermal Thellier-type experiments using the IZZI protocol, with the thermal plots showing the highlighted temperature steps (°C) and the microwave plots showing the highlighted power steps (W.s, Watts per second). The thick black lines connecting measurement steps are the pTRM checks. The k' value is the curvature of the selected component on the Arai plot (49). The corresponding orthogonal plots are inset in the top right corners of the Arai plots. Plots (a-b) are examples from the sites where there are only thermal measurements as the components come from both the magnetite and hematite temperature ranges (Fig. S2a). The remaining plots (c-f) come from the magnetite (Fig. S2b) only samples and show microwave and thermal examples from sites that have similar hysteresis properties (Fig. S2e), WB2-WB3 (c-d) and WB4-WB5 (e-f).

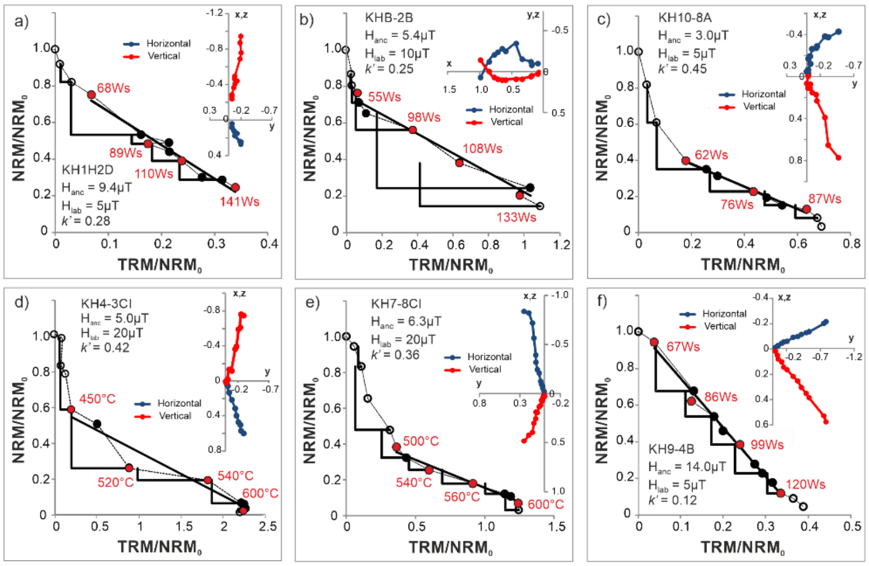

Figure 3. Representative Arai plots from six of the Kinghorn sites a) KH1, b) KHB, c) KH10, d) KH4, e) KH7 and f) KH8/9, illustrating the different Arai plot behaviors observed. All the measurements were done using microwave and thermal Thellier-type experiments using the IZZI protocol, with the thermal plots showing the highlighted temperature steps (°C) and the microwave plots showing the highlighted power steps (W.s, Watts per second). The thick black lines connecting measurement steps are the pTRM checks. The k' value is the curvature of the selected component on the Arai plot (49). The corresponding orthogonal plots are inset in the top right corners of the Arai plots. All the Arai plots represent (low-Ti titano-)magnetite apart from a) KH1 and b) KHB.

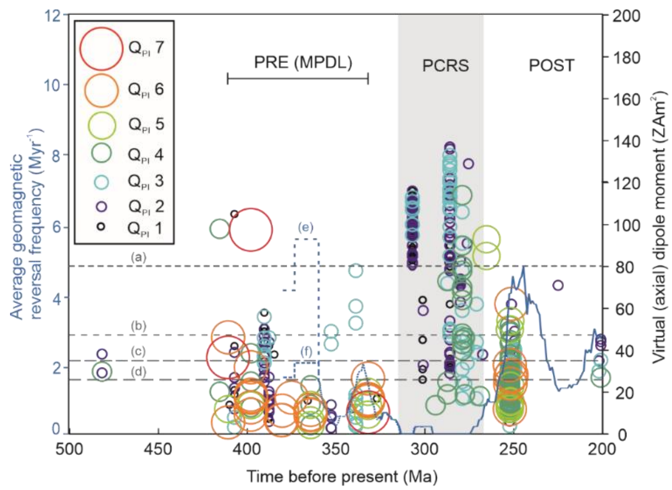

Figure 4. The age distribution of all the V(A)DM values with Q_{PI} >0 between 200–500 Ma. A summary of the Q_{PI} scores applied to each of the studies from this period are outlined in Datasets S3 and S4. The size and the color of the circles representing the V(A)DM values corresponds to the Q_{PI} scoring as outlined in the key. The PRE-, PCRS, and POST- section refer to the same age bins used for the Kolmogorov-Smirnov tests in Figure 5 and Table S2. The dashed lines represent a) the present day field strength (50), b) CNS at Q_{PI} ≥3 (16), c) JHAP Q_{PI} ≥3 (16), d) JHAP Q_{PI} ≥0 (16), e) the maximum possible and f) the minimum possible reversal frequency from the Canning basin magnetostratigraphy (46).

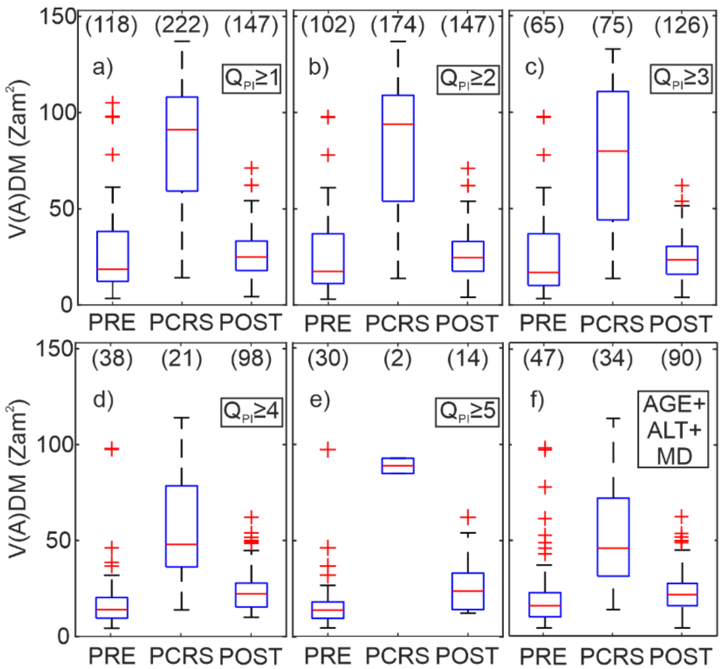

Figure 5. Boxplots showing the V(A)DM distribution of the PRE, PCRS and POST bins (same as in Table S2). The boxplots are filtered based on the total Q_{PI} scores applied to the sites, between Q_{PI} ≥1 to Q_{PI} ≥5 (a-e) and for sites that pass the AGE, ALT and MD criteria (f). The numbers over the boxes display the number of sites in each of the age bins. On each box, the central mark is the median, the edges of the box are the 25th and 75th percentiles, the dashed lines extend to the most extreme data points not considered outliers, and outliers are plotted individually (+).

Table 1. Summary of paleointensity results and Q_{PI} scores for all the Strathmore and Kinghorn sites.

	Strathmore						**Kinghorn**							
Site	CB1	SN1	WB1/2	WB3	WB4	WB5	KH2	KH1	KHA	KHB	KH 10	KH4	KH7	KH8/9
<u>Paleointensity results:</u>														
n_{INT}	9	11	22	12	15	13	20	28	12	21	17	10	12	23
N_{INT}	5	5	11	7	5	2	6	12	3	9	4	6	4	9
N_T	5	5	8	3	2	1	1	1	-	1	-	2	1	-
N_{MW}	-	-	3	4	3	1	5	11	3	8	4	4	3	9
mean (μT)	50.9	12.6	16.8	19.7	3.1	6.3	6.6	6.1	3.7	6.7	5.2	5.3	10.9	8.6
s.d. (μT)	15.9	3.6	5.8	6.4	0.3	4.3	3.0	1.6	0.5	2.5	1.1	0.7	4.3	4.0
s.d./ mean (%)	31	29	34	32	10	68	45	26	13	38	22	13	40	47
VDM (ZAm^2)	**98.0**	**20.2**	**36.6**	**46.2**	**5.6**	**12.0**	**16.4**	**15.7**	**9.3**	**16.8**	**13.4**	**10.4**	**26.6**	**20.2**
<u>Q_{PI} scores:</u>														
AGE	1	1	1	1	1	1	1	1	1	1	1	1	1	1
STAT	0	0	0	0	1	0	0	0	0	0	0	1	0	0
TRM	0	0	1	1	1	1	1	1	1	1	1	1	1	1
ALT	1	1	1	1	1	1	1	1	1	1	1	1	1	1
MD	1	1	1	1	0	0	1	1	1	1	1	1	1	1
ACN	1	1	1	1	1	1	1	1	1	1	1	1	1	1
TECH	0	0	1	1	1	1	1	1	0	1	0	1	1	0
LITH	0	0	1	0	0	0	0	0	0	0	0	0	0	0
MAG	1	1	1	1	1	1	1	1	1	1	1	1	1	1
Q_{PI}	**5**	**5**	**8**	**7**	**7**	**6**	**7**	**7**	**6**	**7**	**6**	**8**	**7**	**6**

n_{INT}: number of samples measured; N_{INT}: number of measurements that passed selection criteria; N_T: number of accepted measurements from thermal IZZI; N_{MW}: number of measurements from microwave IZZI; s.d.: standard deviation; VDM: virtual dipole moment. The nine Q_{PI} are described in full in Biggin and Paterson (27), 1 is a pass and 0 is a fail to meet the qualitative criteria, and Q_{PI} is total score of all these criteria. Site longitude, latitude and the corresponding site directions are available in Table S2.

Supplementary Information Text

Geological Background and Sampling

Strathmore Locality. The older of the northern UK localities is part of the Lower "Old Red Sandstone" suite of the Strathmore region, from the northern Midland Valley in Scotland (Fig. 1). This succession is represented by interbedded fluvial conglomerates and sandstones, punctuated by calc-alkaline volcanism, and was deposited as part of three successive, graben bound sedimentary basins: the (a) Stonehaven (Stonehaven Group), (b) Crawton (Dunnotar-Crawton Group), and (c) Strathmore (Arbuthnott–Garvock and Strathmore Groups) basins (1). The magmatism originates from the subducting Laurentian plate under the Iapetus suture (2) and was greatest during the deposition of the Dunnotar-Crawton Group to the Lower Arbuthnott–Garvock Group. The basaltic lava flows of the Crawton Volcanic Formation (VF; Crawton Group) and the Montrose and Ochil Hill VF's (Arbuthnott Group) provided the material for this study and for the paleomagnetic pole (3).

Published Rb-Sr age dates exist from units correlated to the Crawton and Ochil Hills VFs, but there is no flow-level age data available. The Lintrathen Tuff Member of the Crawton VF has been correlated to the Glenbervie Porphyry member north of the highland boundary fault, which has been dated using Rb-Sr (4) and recalculated to 415.5 ± 5.8 Ma (5). For the Ochil Hills Volcanic Formation, Rb-Sr age dating was done on rhyolite from the base of the Wormit Bay section (4) and recalculated to 410.8 ± 5.6 Ma (5). This age agrees closely with misopore assemblages from the sedimentary rocks of the Wormit Bay section to the Lockhovian (419.2 ±3.2 Ma to 410.8 ± 2.8 (6)). No isotope age date exists for the Montrose Volcanic Formation, although it has been correlated with ignimbrite situated 120 m stratigraphically above the top of Crawton lavas (1) and lies below the Ochil lavas.

Paleodirections from the Strathmore region were originally measured by Sallomy and Piper (7) to determine the Devonian pole for Britain, which was later superseded by the paleomagnetic pole determined by Torsvik (3). Torsvik (3) found that the complex spread of the directions of the original study could be largely explained by the demagnetization techniques used, with peak alternating field (AF) values of ~30-50 mT (considered low by modern standards), and local tectonics. Torsvik (3) also reported two groups of directions. The Group 1 directions are similar to those from Sallomy and Piper (7) and are considered primary, based on the nearly antiparallel normal and reversed directions and passing fold tests and conglomerate tests on samples from below flows 1 and 4 from the Crawton VF (Crawton Bay). Furthermore, samples taken from the conglomerate near the contact with flow 1 (within 0-0.5 m) gave similar directions to the overlying flow, suggesting they might pass a baked contact test. The Group 2 directions were only observed at 3 sites (including two from Crawton Bay); however, despite coming from the highest temperature component, these near-horizontal directions were interpreted to be due to remagnetization (see *Strathmore results: Rock Magnetism* for further discussion).

The paleomagnetic pole, determined only from the Group 1 directions, has a quality (Q) factor of seven (8, 9), which evaluates whether seven qualitative criteria that affect the reliability of the paleomagnetic pole were addressed in the study. However, the data indicate that the locality mean directions (Table III; Torsvik (3)) were calculated with all the specimen-level measurements having the same weighting, which is inconsistent with modern methods for determining the locality mean directions. To compare the locality mean directions from Torsvik (3) to those from this study, first the site means were calculated from the Group 1 directions (Table II; Torsvik (3)), before then averaging these to get the locality mean. There is a <2.5° difference between these revised normal, reverse and combined mean directions and the original Torsvik mean directions (although the k values are no longer artificially inflated by the high N values). The updated directions are included in this summary table (Table S1), along with the site mean results from this study. A common true mean direction (CTMD) test was used (as a reversal test) to check that the distributions of site mean directions were antiparallel came back positive at classification C (Angle = 7°, Critical Angle = 17° (10–12)). In addition to the paleodirectional work, there has also been a paleointensity study (13), which used some of the same samples as the original paleodirectional study (7), including some of those considered 'transitional.' However, questions regarding the reliability of the results (outlined in *Motivation*) indicated that revisiting this locality was worthwhile.

Sampling was done with the intent to closely mimic the sites locations used for the paleomagnetic pole (3), but precise matches were not always possible because of the limited information published about the site locations. Of the locations sampled (Fig. 1), the Crawton Bay and Todhead flows (Crawton VF) are the same as those used for the published pole, the Scurdie Ness sites (Montrose VF) are from roughly the same location, while the Wormit Bay (Ochil Hills VF) sites (14) are likely new sites, though they seem to be located close to the Tayside site, based on the map from Torsvik (3). Samples were collected from five lava flows from the Crawton VF (Crawton Bay and Todhead; CB1-CB4 and TH1), three from the Montrose VF (Scurdies Ness; SN1-SN3) and four from the Ochil Hills VF (Wormit Bay; WB2-WB5) for a total of twelve potential sites. All were visually distinct lava flows, apart from the Scurdie Ness lava flows (the boundaries were not clearly visible in the field), where sites were taken substantial distances (i.e. >100 m) from each other. Samples were also collected from a baked sediment (WB1; underlying the WB2) for a baked contact test and from clasts within the conglomerate at Todhead (TH2; underlying TH1) for a conglomerate test. Most of these samples were collected as oriented drill cores, while the rest were collected as oriented hand samples, such as CB3-CB4, SN2, WB1. Attempts were made at collecting sun compass readings, although weather conditions largely prevented it; the few available readings were largely consistent with the magnetic readings, so all the samples were oriented using magnetic readings for consistency. Tilt corrections were applied from readings from sedimentary units (WB1 and a sandy layer within TH2) or from clear flow boundaries.

Kinghorn Locality. The Kinghorn Volcanic Formation, part of the Visean volcanic sequences of the Midland Valley, near Kinghorn, Scotland (Fig. 1), provided the second sample set. This formation comprises a thick sequence (~485 m) of lava flows interspersed with minor thin intercalations of sedimentary and volcanoclastic layers (15). These lava flows are predominantly olivine basalts, which approach picrite compositions in some areas (16). Thirty flows have been mapped in the region, dipping moderately (20-30 degrees) to the NE, and ranging in thickness from 2.5-12 m. Magmatism in this region is thought to be the result of lithospheric extension caused by the Variscan front to the south, which also led to rifting and the development of fault-bound basins.

Stratigraphically, the age of the Kinghorn lavas are well constrained by correlations to the Sandy Craig and Pathead Formations of the Strathclyde Group, whose strata are found above and below, as well as interbedded with the Kinghorn Volcanic Formation (17). The misopore assemblages in these correlated sedimentary rocks constrain the age of the Kinghorn lavas to the Asbian-Brigantian (~337.5-326.4 Ma (17)). Isotopic age dating has been largely unsuccessful, generally underestimating ages, possibly due to Argon loss (18). The closest isotopic age date to the Asbian-Brigantian comes from a K-Ar age date of 338 ± 4 Ma from a sample collected between Burntisland and Kinghorn (19) but, as the paleontology appears more robust, the mean stratigraphic age is used (332.0 ± 5.6 Ma) in this study.

The Kinghorn locality has only one prior paleomagnetic study; its paleomagnetic pole, which was determined by Torsvik et al. (20), has a Q factor of 6 (8, 21). This study has a lower Q score then the Strathmore paleomagnetic pole because field tests were not performed. However, the directions from the Carboniferous lavas agree with the high temperature component from the underlying Old Red Sandstone (ORS) units, which is due to remagnetization of the ORS based on the negative fold and conglomerate tests and it being a local feature (the primary direction is found elsewhere in the ORS). As with the Strathmore locality, the aim was to sample as close to the original sites as possible, but as with the Strathmore sites, identical sampling was difficult due to the limited published information. Samples were collected from eleven distinct lava flows from the Kinghorn locality; nine sites (KH1-KH10; KH8 and KH9 were later recognized to be a single flow/site (KH8/9)) were collected on the first trip and two from a later trip (KHA-KHB). For the Kinghorn (KH) sites, one site was collected on Burntisland (KH2), and the rest were collected between Pettycur Harbour and Kinghorn Harbour (KH1, KHA-KHB, KH3-KH10). The majority of samples were collected as oriented drill-cores, while the rest were collected as oriented hand samples (KH1-KH2, KHA-KHB, and the odd sample from other sites) that were then drilled in the laboratory. Most core samples were oriented using sun compass readings, with a few oriented using magnetic readings if they were hand samples or sun readings could not be taken (the two readings were generally consistent with each other). Tilt corrections were applied from readings taken from clear flow boundaries and sedimentary interbeds.

Methods

Paleodirections. All the paleodirections were obtained using stepwise thermal demagnetization. About half of these measurements (most of the samples from KH3-KH8/9, TH1-TH2 and WB2-WB5) were made using full 2.5cm cores, heated in the 24-sample Magnetic Measurements Thermal Demagnetizer (MMTD24) and measured using an Agico JR6 Spinner magnetometer. The rest came from half-height 2.5cm cores that were heated in a Super Cooled MMTD(SC) and measured on a RAPID 2G SQUID magnetometer (22). Samples were progressively heated to a maximum temperature between 580-680 °C, when the remaining magnetic intensity of the sample had decreased to <10 % of the natural remanent magnetization (NRM). The high temperature magnetic components, interpreted as the Characteristic Remanent Magnetization (ChRM), were selected based on the orthogonal plots and calculated using principle component analysis (PCA (23)). If the mean angular dispersion (MAD°) and the angle between the anchored and unanchored directions (α°) of the individual directions were ≥15°, these directions were not included in the site mean analysis. Sites with dispersed, non-clustering paleodirections (k <15) were also excluded from further analysis (see Table S1). These site means are not intended to supersede previous paleomagnetic studies (as many of the site N values are fairly low) but rather to determine if the sites can reliably be used for paleointensity.

Rock Magnetism. To broadly determine these sites' magnetic mineralogy, rock magnetic analysis was performed on representative specimens from each site. Hysteresis loops, isothermal remanent magnetization (IRM) and back-field IRM curves, and thermomagnetic (Curie) curves were run in air on crushed specimens on a Magnetic Measurements Variable Field Translation Balance (MMVFTB). The thermomagnetic curves are used for categorizing the types of magnetic minerals present in the samples based on the Curie temperatures (T_c) indicated, whether the minerals appear to alter and, if so, over what temperature range. Determining the magnetic mineralogy helps identify whether the sample is likely to carry a primary TRM. However, the magnetization is often dominated by the larger of the population of magnetic grains in the sample, which are unlikely to be the primary remanence carriers and so the irreversibility of these curves is not a good indicator for how low-temperature alteration of the NRM might affect the paleointensity experiments (see *Methods: Paleointensity (SI*) for details on the alteration checks used instead). The hysteresis and IRM measurements are used as indicators of the bulk grain size distribution.

Scanning electron microscopy (SEM) analysis was also performed on representative sites with accepted paleointensity results using a Hitachi Table-top Microscope TM3000. Back-scattered electron (BSE) images of representative thin sections were used to confirm the presence of igneous textures, consistent with the samples carrying a primary thermoremanent magnetization. This analysis included looking for textures that are consistent with the rock magnetic results, such as exsolution lamellae, euhedral vs. skeletal structures, etc., and for any cracking of magnetite grains that could be consistent with a volume reduction of the grains due maghematization, which would result in a thermochemical remanent magnetization (TCRM) that is not suitable for paleointensity experimentation. Energy-dispersive X-ray (EDX) analysis was used, in conjunction with the BSE images, to assist in the identification of the magnetic mineralogy.

Paleointensity. Sites were deemed suitable for paleointensity analysis if they a) passed the paleodirectional selection criteria, b) had directions consistent with previous studies, and c) produced rock magnetic results that were not inconsistent with a primary TRM. Two paleointensity techniques were applied to specimens from these sites: thermal and microwave Thellier-style experiments using the “IZZI” protocol (24), starting with a zero-field (Z) step. Partial TRM (pTRM) checks (25) were used to check that the remanence carriers did not alter due to heating during the experiment. Thermal experiments used oriented 2.5 cm diameter core specimens (~1 cm in height), heated in air in the super cooled MMTDSC and then measured on the RAPID 2G SQUID magnetometer. A field of 20 µT was applied along the core’s Z-axis for the in-field (I) steps. An alternating field (AF) step of 5 mT was applied before measuring each heating step, as an ‘AF cleanse’, in order to reduce any potential non-single domain (SD) effects, such as pTRM tails (26), on the paleointensity estimate (27, 28). Temperature steps were determined from the behavior of sister specimens from thermal demagnetization and the rock magnetic data. An initial temperature of 300 °C was selected to avoid the low temperature overprints observed in the paleodirection data. Steps of 20–50 °C were used to a maximum of 600–660 °C, depending on the magnetic mineralogy.

Microwave experiments were performed on unoriented 5 mm diameter cores that were both (de)magnetized and measured in air using the “Tristan” 14 GHz microwave SQUID magnetometer system at the University of Liverpool (29). Each microwave specimen is run individually, so a field of 3–20 µT, calibrated using other paleointensity estimates from each respective site, was applied, at an angle of 45–90 ° to the NRM. The selection criteria used in this study (provided in Datasets S1 and S2) are comparable to those used in recent studies of a similar age from Siberia (30, 31), but with a stricter FRAC cut-off used for this new study. The FRAC value (≥0.35) is still lower than recommended (32); however, these suggested criteria are based on single component Arai plots. A larger FRAC value is used here because, on average, the overprint on these samples represents a smaller part of the NRM than the other studies and it reduces the misfit of the site mean data, while enough estimates are accepted to still be statistically rigorous.

Strathmore Results

Paleodirections. Out of the 100 samples from the 12 sites that were thermally demagnetized (this does not include WB1 and TH2, which were used for field tests), 90 passed the paleodirection selection criteria. All the sites had N ≥3 directions and representative orthogonal plots (Fig. S1ai-di), with corresponding intensity curves (Fig. S1aii-dii), from accepted measurements show that the NRM is made up of potentially three distinct components. The data indicate a low temperature component between 0-100 °C (likely a viscous remanent magnetization; VRM), a mid-temperature component, and the high-temperature component, which is considered to be the ChRM, from around ~340-480 °C and to 600-680 °C. The different unblocking temperature ranges for the different sites reflect the different magnetic mineralogies observed (see *Strathmore Results: Rock Magnetism* for further details). All the measurement data is included in the MagIC database (https://earthref.org/MagIC/17067).

For these 12 sites, all but one of the site-mean directions (SN2) were reasonably well-clustered with k >15 (Table S1) and covered both the normal and reverse field states (Fig. S2a). Both the normal and reverse directions from this study agree fairly well with the revised mean directions from Torsvik (3), with angular differences of 7.8° and 10.7° respectively and substantial overlap of their respective α_{95} circles. From the Crawton Bay flows, only CB1 has a reversed direction, which suggests that it is the same as flow 4 from the Torsvik study (3), with flows 1, 2, and 3 being CB3, CB4, and CB2, respectively, based on their relative positions. Interestingly, sites CB3-CB4 lack a shallow, high-temperature component (Fig. S1ai) consistent with the Group 2 directions from Torsvik (3), despite showing them in the original study; however, this remagnetization was only recorded in some of their samples. A conglomerate test was performed on a new site, the conglomerate overlying TH1 (site TH2), which showed that the directions are uniform with weak support (Fig. S2b; $P(H_A|R) = 0.71$ (33)). The random nature of these directions suggests that the conglomerate has not been remagnetized, but the degree of confidence is limited by the low number of samples used (n = 8). A baked contact test was also performed, using a CTMD test between the directions from the baked sediment at Wormit Bay (WB1) and the overlying lava flow (WB2), which was positive at classification C (Angle = 7°, Critical Angle = 10° (10–12)).

Rock Magnetism. The magnetic mineralogy of the Strathmore sites can be divided into four types; the first of which produced rock magnetic results consistent with 'Type B' magnetic mineralogy from the Torsvik study (3). These sites (CB2-CB4, TH1 and SN3) gave thermomagnetic curves that are largely reversible up to 300 °C but then show a ~30-40% decrease in magnetization between 300-600 °C and provide Curie temperatures (T_c) of ~470–540 °C (Fig. S3a), apart from TH1, which produced a T_C of ~620–640 °C. These results are consistent with the presence of (titano-)maghemite, which converts into (titano-)hematite when heated above 300 °C. The presence of (titano-)maghemite suggests that these sites underwent chemical alteration after the lavas were emplaced (maghemite is not an original, or primary, mineral in lavas) and may carry a TCRM (12). Also, as (titano-)maghemite is only metastable (12), it is likely that some of it may have inverted into hematite at some point during the history of the sites, which may explain the high-temperature, near-horizontal directional components categorized as the Group 2 directions (3).

The other three magnetic mineralogy types produced thermomagnetic curves that generally showed greater reversibility (≤20% decrease in magnetization when heated to 600-700 °C) then the Type B curves. The curves from sites CB1 and SN1 show two apparent values of T_C (Fig. S3b), the first at ~580 °C, indicative of magnetite, and the second at ~680 °C, indicative of hematite. This curve is consistent with the Type C curves from Torsvik (3). Hematite can be a primary magnetic mineral in igneous rocks but is also produced by alteration (12). As the paleodirectional component is from a temperature range that is consistent with both the magnetite and hematite temperature ranges (340-680 °C; Fig. S1bi), both are likely primary minerals. These sites plot in the upper part of the bulk domain stability plot in Fig. S3i, trending above and perpendicularly away from the bulk domain stability (BDS) line (34), which is consistent with the presence of hematite. There is no SEM analysis available for samples of this rock magnetic type.

The thermomagnetic curve (Fig. S3c) and hysteresis properties (Fig S3i) for the baked sediment (WB1) are similar to those from CB1 and SN1 because WB1 has a Tc consistent with hematite (~680 °C) but not magnetite. The hematite component likely carries a primary TRM since its direction is consistent with the overlying lava. The last mineralogy type (sites WB2–WB5) had associated thermomagnetic curves with values of T_C from 520-580 °C (Fig. S3d), which corresponds to the (titano-)magnetite Type A curves from Torsvik (3). SEM analysis of the samples showed grains of low-Ti (titano-)magnetite next to ilmenite, both on the order of tens of µm in length, with no finer exsolution structure apparent (Fig. S3g). All these samples plot near but just above the 'BDS trend' line (Fig. S3i).

Kinghorn Results

Paleodirections. Out of the 57 samples, from 9 sites sampled, that were thermally demagnetized for paleodirections (KH8/9 were combined into a single site and KHA-KHB were not included in the paleodirectional analysis), 47 passed the paleodirection selection criteria. Three sites failed to produce consistent directions (KH3, KH5-KH6), because of both individual directions failing to pass the selection criteria and the site directions not clustering, which may relate to the magnetic mineralogy of the samples (see the *Kinghorn; Rock Magnetics* section). Representative orthogonal plots (Fig. S1ei-fi), and corresponding intensity curves (Fig. S1eii-fii), from accepted measurements indicate a possible VRM between 0-100°C and a small mid-temperature overprint (the intensity of these overprints combined is <25% of the NRM), before the ChRM, which generally starts at 300-480 °C and finishes between 540-600 °C, depending on the titanium content of the sites (see *Kinghorn; Rock Magnetics* section for further details).

Of the accepted paleodirectional sites from this study, the majority of the lavas sampled here are normal in polarity (four of the six; Table S1 and Fig. S2c), unlike Torsvik (20), which sampled more reversed polarity lavas to the north of those herein. The mean normal polarity direction from this study agrees well with that from Torsvik, with <3° angular difference. The mean reverse direction from this study is very poorly constrained (α_{95} >100°) because the paleodirectional sites (KH1-KH2) also only have N = 2, while the other two reversed sites (KHA-KHB) were not included in the paleodirectional analysis because they only have a single oriented hand sample each. However, the directions from both the paleodirectional sites (especially KH2) and from oriented paleointensity measurements (which both lie within the α_{95} circle of KH1) are also sufficiently similar, given the low N (n) values, to the mean reversed direction from Torsvik (20) to be considered for paleointensity analysis (Fig. S3c; there are no individual site directions from Torsvik (20) to compare against, which might have agreed better). All the measurement data are included in the MagIC database (https://earthref.org/MagIC/17067).

Rock Magnetism. The majority of the Kinghorn sites that gave acceptable paleodirections (KH2, KH4 and KH7-KH8/9) produced thermomagnetic curves similar to the Type A curves from Torsvik (3), with a T_C range from ~540–580 °C, indicative of low-Ti (titano-)magnetite (Fig. S3e). Sites KH1, KH10 and KHA-KHB, as well as all the sites that failed to give acceptable paleodirections, gave substantially lower T_C's in the range of 370–480 °C (the lowest values came from the sites that failed to pass paleodirection selection criteria; KH3 and KH5-KH6). These curves showed an increase in magnetization when heated above ~500°C (Fig. S3f), which is indicative of the formation of magnetite from exsolution of the titanium-rich titano-magnetite upon heating. SEM analysis indicates the presence of very coarse exsolution structures between the titanomagnetite and ilmenite phases (Fig. S3h), with the titanomagnetite forming around the edge of large, skeletal grains of ilmenite (hundreds of µm in length). All the sites plot close to the BDS trendline, with moderate M_{rs}/M_s and H_{cr}/H_c values, apart from KHB, which has the lowest T_C (indicating moderate-Ti titanomagnetite), which may have affected its BDS value (Fig. S3j).

Paleointensity Reliability Assessment

Q_{PI} criteria. While selection criteria, such as those used in this study (see Datasets S1 and S2), are designed to check the reliability of measurements at the specimen level, there are also a number of factors that can affect the reliability of paleointensity estimates that are not evaluated by these criteria. To assess these site-level factors, Biggin and Paterson (35) outlined a set of nine quality criteria for paleointensity (Q_{PI}). These criteria emulate the Quality (Q) criteria outlined by Van der Voo (9), which are used to assess the reliability of paleomagnetic poles, and are scored the same way (a pass = 1, fail = 0 and the Q and Q_{PI} scores are the total of all the criteria scores). An overview of how these nine criteria have been assessed in this study is outlined here:

1. AGE: This criterion requires that the site has a reliable age constraint from either radiometric or stratigraphic age dating, with errors that are less than 10% of the age. Corresponding paleodirections are not required to pass this criterion because this can discriminate against materials that are difficult to orient but otherwise have good age constraints (i.e. some ocean drill cores, single crystals, etc.). However, where they are available, the directions should not unquestionably deviate from what is expected from the age of the sites (transitional sites and sites where the apparent polar wander paths are not well constrained would still pass). This includes whether normal and reverse directions are observed i.e. sites age dated to a superchron should not include reversals and vice versa.
2. STAT: This criterion assesses the consistency between paleointensity estimates from the same site as there is no geomagnetic reason for discrepancies between samples that acquired their TRM in the same field. To pass STAT, the site mean must be calculated from at least 5 specimens (N ≥5) and the standard deviation (std.dev.) of these measurements, normalized by the site mean (std.dev./mean), must be ≤25%. However, because the N values for paleointensity studies tend to be statistically small, there are high levels of uncertainty associated with the std.dev. and mean and so the upper 95% confidence interval should be used (δB_N% (36)) to ensure a std.dev. ≤25% (for N = 5 at 25% maximum, δB_N% = 15.97%).

3. TRM: This criterion recognizes that, while the effects of chemical alteration may be identifiable from rock magnetic techniques, microscopy is well suited to identify clear occurrences of low-temperature alteration that may otherwise be missed. In the majority of cases, the study must present evidence for primary igneous textures that are consistent with TRM acquisition and no apparent alteration to pass this criterion. There are some exceptions to this, such as when the remanent magnetization is unlikely to have been acquired by any means other than thermally (i.e. where the magnetization is held by inclusions in silicates (37)) or there is other compelling evidence for thermal acquisition (i.e. a baked contact with consistent paleodirections as the igneous body).
4. ALT: Alteration of the magnetic carriers can present a major issue for the reliability of paleointensity estimates as they are calculated assuming that the magnetic recorders have remained unchanged between ChRM and (lab induced) TRM acquisition and almost all conventional paleointensity techniques include at least one heating step (38). To pass the ALT criterion, measurements should include some form of alteration check. This is generally pTRM checks for Thellier-type experiments (25), while other methods, such as the Shaw method (39), pass by comparing ARM acquisition before and after heating. Ideally, some selection criteria relating to these checks should be applied to the measurements; however, the type of criteria should not be taken into consideration, unless it has shown to be completely ineffective at detecting alteration. The main exception to this is if the paleointensity experiment includes no heating step (i.e. calibrated pseudo-Thellier (40)), it will automatically pass ALT.
5. MD: It is well established that the behavior of multi-domain (MD) grains (as well as interacting grains, which have been shown to behave in a similar way (41)) can affect the paleointensity estimate. For any paleointensity experiments using pTRMs (i.e. Thellier-type experiments), MD behavior is expressed as tails, causing the Arai plots to "sag" or "curve" below that of the linear behavior expected from SD grains (26, 42). Site values from Thellier-type experiments can pass this criterion if the experiment includes some protocol for checking for MD effects during the experiment. This includes pTRM tail checks (43), checking for curvature of the selected component (e.g. $|k|$ *or* $|k'|$ (44)) or using the IZZI protocol (24), where pTRM tails are expressed as zig-zagging in the Arai

and/or orthogonal plots (the site will only pass if the selected components lack a clear indication of zig-zagging). The site may also pass if the selected component is from linear, single component Arai plots, which can be determined from selection criteria e.g. high f or FRAC values, which indicate that the Arai plot is near single-component, and low β values that suggest the component is linear (see Standard Paleointensity Definitions (SPD) for details (45)). Other techniques, such as the Shaw (39) and Wilson (46, 47) methods, automatically pass the MD criterion as they are considered to be domain-state independent. Bulk hysteresis measurements that are consistent with the "pseudo-single domain" grains (48) are insufficient to pass the MD criterion as domain state effects can still be an issue (49)

6. ACN: This criterion is divided into three sub-criteria, reflecting three issues that can bias paleointensity estimates but are not as commonly observed with paleomagnetic sites as ALT and MD and are correctable. While the sub-criteria are combined into a single Q_{PI} criterion, so that their weighting is kept proportional in comparison to the other criteria, all the sub-criteria need to pass for the site to pass ACN (if one fails, the site fails ACN). These sub-criteria are:
    a. Anisotropy of TRM: This is not commonly an issue for paleointensity (i.e. igneous) targets, but it has been shown to be an issue for some localities (50). Experiments using an applied field parallel to the direction of the ChRM would pass this sub-criterion automatically. Otherwise, checks that show that anisotropy of TRM is not affecting the paleointensity estimates, would be accepted. An acceptable check is a low gamma (γ) value (51), i.e. the angle between the applied field and last pTRM acquired for the selected component. Anisotropy of ARM experiments could also be used to show that anisotropy of TRM is not an issue for the site (52). The site can still pass if anisotropy of TRM is an issue if an appropriate correction has been applied (50, 53).
    b. Cooling rate effects: It has been shown both theoretically (54, 55) and experimentally (56) that the TRM acquired by SD grains is greater when slow-cooled, rather than fast-cooled. This can bias paleointensity estimates because there are normally several orders of magnitude difference between the cooling

rates in nature and the lab. Studies suggest that this should only really be an issue when the remanence carriers are SD in size (57–59) or are within a large intrusion that has cooled over hundreds of thousands of years. In general, “fast-cooled” igneous sites (e.g. lavas and smaller dykes and sills) pass this sub-criterion as the remanence carriers are normally larger than SD grains (preferably this would be supported by rock magnetic data such as bulk hysteresis measurements though). It may also be possible to check for cooling rate effects if the site includes measurements from different techniques with substantially different cooling rates (the faster the cooling rate in the lab, the higher the paleointensity estimate should be). For materials that carry SD grains or slow-cooled sites (e.g. plutons and larger sills), a cooling rate correction needs to be applied (54, 55) for the site to pass this sub-criterion. It is also worth noting that there has been recent work that suggests that cooling rates may affect more paleointensity measurements with non-SD carriers more than previously considered (60). However, further work is needed to quantify how this may have affected the paleomagnetic record, especially as there is potentially no way to correct past studies as there was no observed correlation between the cooling rate dependence and commonly measured magnetic properties (i.e. bulk hysteresis).

c. Non-linear dependence of TRM: An assumption when calculating paleointensity estimates is that the relationship between field strength and TRM acquisition is linear at weak (Earth-like) field values. However, for some magnetic grain assemblages, non-linear TRM acquisition can occur at sufficiently low field values that it affects either NRM or lab TRM acquisition (61). If the applied field during a paleointensity experiment is the same or close (within 1.5x of) the field the NRM was acquired in, then the effects of non-linear TRM dependence should be negligible and the site passes this sub-criterion. Sites with low field values for both the applied field and the paleointensity estimates (≤60 μT) will also pass as they should both be within the linear portion of TRM acquisition based on experimentation (61). The site may also pass if measurements using substantially different applied field values give consistent paleointensity results.

7. TECH: A multitude of paleointensity techniques have been developed over time, and having accepted results from different methods can provide greater confidence in the results. To be considered different techniques, they should use significantly different styles of unblocking. For example, Thellier-type experiments, all using pTRMs but different protocols, would be considered a single technique but experiments using total TRM acquisition (46, 47) or unblocking grains using the microwave system (62) or AF (39) would be considered separate techniques. The results do not have to be consistent because this requirement is covered by the STAT criterion; however, variation between the techniques may illustrate issues relating to some of the other (sub-)criteria. Consistency between results from more than one technique can also allow sites to pass criteria that using one technique alone would not pass (e.g. sites with consistent Thellier and Wilson can pass MD because Wilson is domain state independent and ALT if there are pTRM checks for the Thellier experiment).
8. LITH: The LITH criterion recognizes that where materials with different lithologies (i.e. materials with substantially different magneto-mineralogy and domain state assemblages) have acquired a TRM in the same field, this can improve the reliability of the site. This scenario is typically only met if there is a baked contact that can be sampled, or an igneous unit has chilled margins and a coarse-grained interior with substantially different mineralogies. There should also be information provided for the magnetic mineralogy of the two units, including evidence for differences in the unblocking temperatures.
9. MAG: This criterion is designed to encourage the publication of the raw measurement data somewhere accessible (such as the MagIC database, which the criterion is named after, but it can be published elsewhere and pass this criterion). Whatever the format/depository chosen, the raw measurement data should allow others to be able to analyze the data for themselves. However, while this criterion has been assessed for all the 200-500 Ma sites in the PINT15 database (Dataset S3), this criterion has not been included in the total Q_{PI} scores used for long-term field strength analysis (Figures 4 and 5

and Table S2) because the publication of the raw measurements is a very recent phenomenon and so this criterion would probably add unnecessary bias to the most recently published studies.

Strathmore Q_{PI} Scoring. The individual site Q_{PI} scores for the Strathmore sites can be found in Table 1, as well as Datasets S3 and S4 (the latter also includes comments on the scoring of the sites). A detailed explanation for the scoring of these sites is included below (numbering of the criteria is the same as in *Paleointensity Reliability Assessment: Q_{PI} criteria* section):

1. AGE: The oldest (Crawton Bay/Todhead) and youngest (Wormit Bay) sites pass AGE because the sections they come from have, or have been correlated with, members that have Rb-Sr age dates (415.5 ± 5.8 Ma and 410.8 ± 5.6 Ma respectively (5)) consistent with the stratigraphic constraints (1) and errors <10% of the age. The Scurdie Ness sites pass because they are stratigraphically between the two other locations and the difference in age between the two sites (including errors) is <10% of the mean age.
2. STAT: None of the Strathmore sites pass STAT. Most of the sites had $N_{INT} \geq 5$ but the normalized standard deviations were too high, possibly because the paleointensity estimates were mostly low (<20 µT), resulting in higher normalized std.dev. However, CB1 had a relatively high site mean value (50.9 µT) and still failed due to scattered paleointensity estimates.
3. TRM: The Wormit Bay sites (WB1/2-WB5) all pass this criterion as the lavas all have similar mineralogy and there are representative SEM images for these sites (Fig. S3h). While WB1/2 represents two lithologies (WB1 is the baked sandstone and WB2 is the lava), and there are no SEM images for WB1, the consistency in paleodirections between the two sites indicates that the baked sandstone was overprinted by the lava. The other sites (CB1, SN1) did not pass this criterion as there is no representative microscopy for them; however, the results are still included because the consistency between the paleodirections and paleointensity estimates from the magnetite and hematite temperature ranges support that their remanence is likely a primary TRM.

4. ALT: All the Strathmore sites passed as all the measurements included pTRM checks and appropriate DRAT/CDRAT selection criteria (see Dataset S1).
5. MD: As the IZZI protocol was used for all the experiments and none of the sites, apart from WB4-WB5, showed any signs of zig-zagging, all the sites (other than WB4-WB5) should pass the MD criterion. Selection criteria to evaluate the curvature of the selected component was also used ($|k'|$ ≤0.48 for all accepted measurements (63)). As for sites WB4-WB5, while they fail this criterion, their low results may not be the result of MD behavior. While the zig-zagging seen in the orthogonal plot obscures it, it is clear from the thermal demagnetization experiments that there are at least two directional components in these sites (see Fig. S1di), and the selected temperature range for the paleointensity estimate (Fig. 2e) corresponds with the temperature range for the ChRM. Also, the curvature of the selected Arai plot components is still low ($|k'|$ <0.31). Finally, a simple estimation of the maximum bias of the paleointensity estimates can be calculated by selecting the first and last (before alteration) points of the Arai plot to see how much it deviates from the theoretical linear, single component plot (although this is unrealistic as the site has clearly been overprinted). The "single component estimates range from ~0.95-2.50x the accepted estimates and, while this seems like a large deviation, in absolute terms it is <9 µT, so the maximum paleointensity estimates would still be <10 µT for WB4 and <20 µT for WB5. This does not change whether the sites pass the MD criterion but is important for the overall consideration of the strength of the field at the time of the Strathmore lavas.
6. ACN: All the Strathmore sites passed ACN because all the sub-criteria were fulfilled:
    a. Anisotropy of TRM: All sites were considered to be unaffected by anisotropy as the locality had a mean γ value of 2.8° (range 0.3-6.7°).
    b. Cooling rate effects: All the Wormit Bay sites, other than WB1/2, pass because they represent relatively fast-cooled lava flows, whose hysteresis properties are consistent with non-SD grains (Fig. S3i, j). The thermal and microwave results from WB4 and WB5 are relatively consistent, despite the difference in cooling rate between the two techniques. There appears to be some difference between the two techniques for sites WB2 and WB3, but the microwave

estimates were generally lower than the thermal estimates, in contradiction with a cooling rate effects (55).The hematite-bearing sites (CB1, SN1, WB1/2) are more likely to be affected by cooling rate because hematite grains tend to be SD in size (64). The measurements from WB1 and WB2 are consistent enough that the site has a negligible cooling rate effect. For the other two sites, reselecting estimates, where the hematite component was included, to just below magnetite's T_C produced estimates within ~15% of those selected from both components and were, in contradiction to the expected effects of cooling rate, generally higher so cooling rate is also unlikely to have affected these sites.

   c. Non-linear dependence of TRM: Both the paleointensity estimates and applied field values were low enough (≤~60 µT) that the non-linearity of TRM should have no significant effect (61).

7. TECH: The Wormit Bay sites (W1/2-WB5) all passed as they included both microwave and thermal experiments. The other sites (CB1 and SN1) do not pass as the microwave system was not able to demagnetize the hematite-bearing sites (this is also true of WB1 but there are microwave experiments for WB2).
8. LITH: Only site WB1/2 passed this criterion as it is the only site with results from two distinct mineralogy's, with distinct unblocking spectra.
9. MAG: All the sites pass as the raw measurement files are included in the MagIC database (https://earthref.org/MagIC/17067).

Kinghorn Q_{PI} Scoring. The individual site Q_{PI} scores for the Kinghorn sites can be found in Table 1, as well as Datasets S3 and S4 (comments on scoring can also be found in Dataset 4). A detailed explanation for the scoring of these sites is included below (numbering is the same as in the previous two sections, *Q_{PI} criteria and Strathmore Q_{PI} scoring*):

1. AGE: The Kinghorn isotopic age dating is generally fairly poor with suspected Argon loss (18). However, the misopore ages from correlated sedimentary sections are well constrained (~337.5-326.4 Ma (17)) and are in close agreement with at least one radiometric age (338 ± 4 Ma (19)), and the difference between the ages is within 10% of the mean age.

2. STAT: Only one site passed the STAT criterion (KH4); three of the sites had N_{INT} ≤5 and the rest had std.dev values that were too high to pass STAT. Like with the Strathmore sites, this may be due to the low site mean values (≤11 μT), meaning that while the absolute std.dev values were low (1.6-4.0 μT for the Kinghorn sites with N_{INT} ≥5 that failed STAT), the normalized std.dev. was relatively high (26-40%).
3. TRM: Based on the rock magnetic measurements, all the Kinghorn lavas are (titano-)magnetite-bearing, with varying amounts of titanium and no evidence of maghematization, so the SEM microscopy (Fig. S3h) should be representative of all the lavas, so all sites pass this criterion.
4. ALT: All the Kinghorn sites passed as all the measurements included pTRM checks and appropriate DRAT/CDRAT selection criteria (see Dataset S2).
5. MD: The IZZI protocol was used for all the experiments and no significant zig-zagging was noted with the Arai or orthogonal plots. Along with the checks for curvature of the selected component (*k'* ≤0.48 for all accepted measurements (63)) there is enough evidence for all the sites to pass the MD criterion. The two-slope Arai plots also are also likely due to overprinting as the orthogonal plots from both the Arai plots (Fig. 3b-e) and those from thermal demagnetization experiments (Fig. S1ei, fi) show the selected component corresponds to the ChRM.
6. ACN: All the Kinghorn sites passed ACN because all the sub-criteria were fulfilled:
    a. Anisotropy of TRM: Unlike for the Strathmore sites, in some cases, γ exceeded 6° for some accepted Kinghorn site mean specimens. This is a cut-off value suggested for isotropic samples based on the work of Paterson (51). AARM experiments were performed on representative samples, using the same methods as described in SPD (45), to investigate this issue further. These gave p values ranging from 1.05-1.19. However, calculating the anisotropic corrections (c values), using the method described in the SPD (45) for some of the most anisotropic sites (KH1, KH4 and KH7; p values of 1.19, 1.16 and 1.12 respectively) gave specimen c values of 0.91-1.10, with a median c value of 0.98, far less than the anisotropy of the specimens themselves. The c values also varied substantially, probably because the c value is dependent on the direction

of the applied field, which was varied for the individual microwave measurements. The site mean paleointensities calculated from the corrected specimen measurements showed negligible offsets from the uncorrected means (corrected site means were 6.0 µT, 5.3 µT and 10.8 µT respectively KH1, KH4 and KH7; the uncorrected site means are in Dataset S2). Due to the limited sample available after the paleointensity experiments, only representative specimens were analyzed. It would not have been possible to correct all the measurements consistently; however, these AARM measurements show that the effect of anisotropy on the paleointensity estimates were negligible, even for the most anisotropic of the Kinghorn sites.

a. Cooling rate effects: All the sites are fast-cooled lavas, and the bulk hysteresis properties show that all the sites plot between the SD and MD regions of the (Fig S2j). Thus, it is unlikely that cooling rate would affect the paleointensity estimates. In addition, the Kinghorn sites produced a slightly lower average paleointensity estimates for the microwave experiments (6.9 µT vs 7.7 µT) than the thermal ones, in contradiction to what is expected from cooling rate effects.
b. Non-linearity of TRM: Both the paleointensity estimates and applied field values were sufficiently low (≤20 µT) that the non-linearity of TRM should have had no significant effect (61).

7. TECH: Five out of the eight sites passed the TECH criterion as they included both successful microwave and thermal Thellier-type experiments, while the three sites that failed only had successful microwave experiments.
8. LITH: None of the site pass LITH as they are all single lithology sites (lava flows).
9. MAG: All the sites pass as the raw measurement files are included in the MagIC database (https://earthref.org/MagIC/17067).

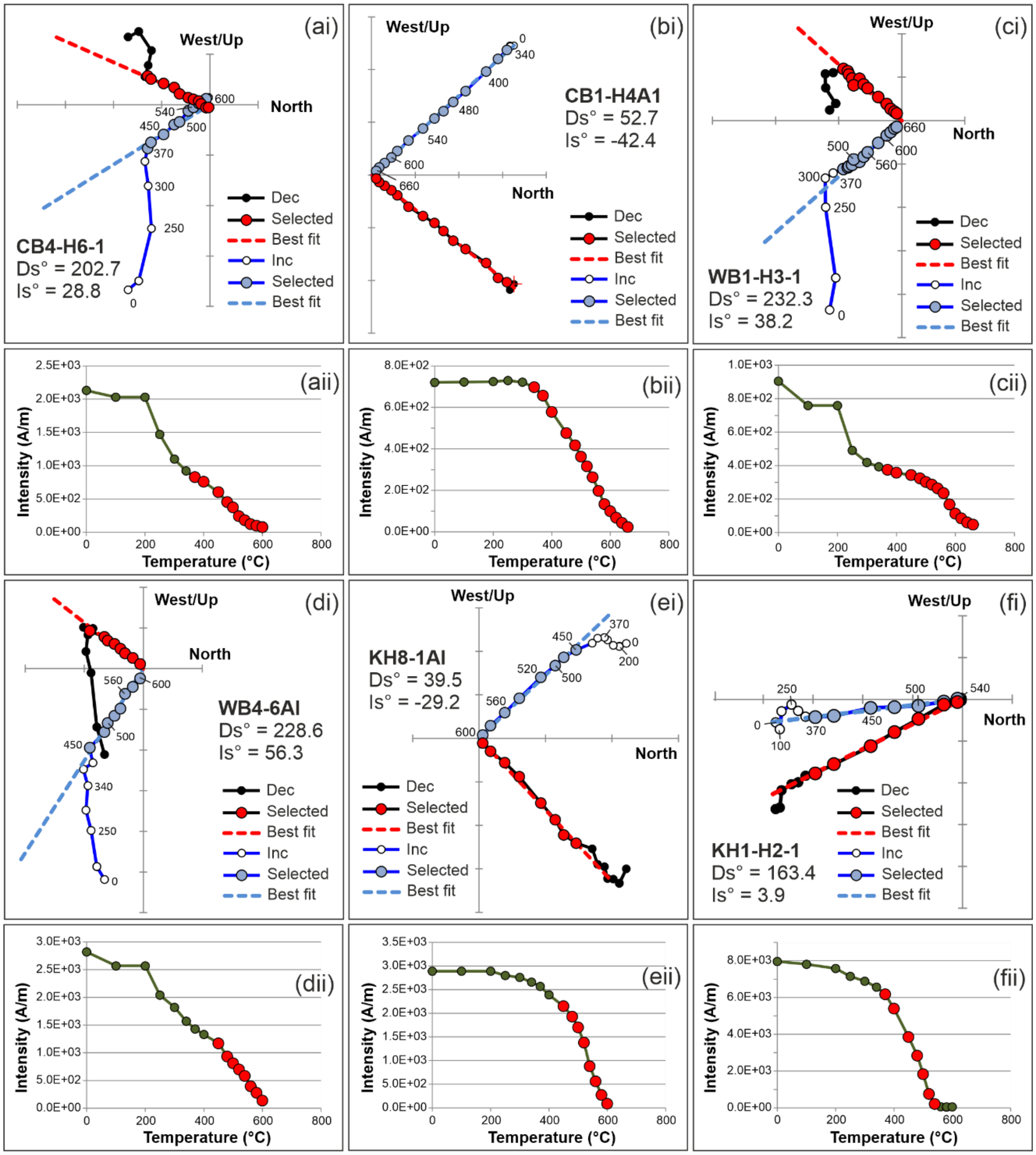

Fig. S1. Examples of i) orthogonal plots and the ii) corresponding intensity curves from the thermal demagnetization experiments from Strathmore (a-d) and Kinghorn (e-f) localities. Each of the examples represents a different magnetic mineralogy (outlined in the *Rock Magnetism* sections from the *Strathmore Results and Kinghorn Results)* and corresponds to the example thermomagnetic curves with the same letter in Fig. S3. Ds° and Is° are the declination and inclination (in stratigraphic co-ordinates) determined from the selected component using PCA analysis (23). The numbers next to the selected points on the inclination curve are the temperature step (in °C). The maximum demagnetization temperatures of the samples are sometimes a bit higher than expected from the corresponding thermomagnetic curves (Fig. S3), which is likely due to thermochemical alteration.

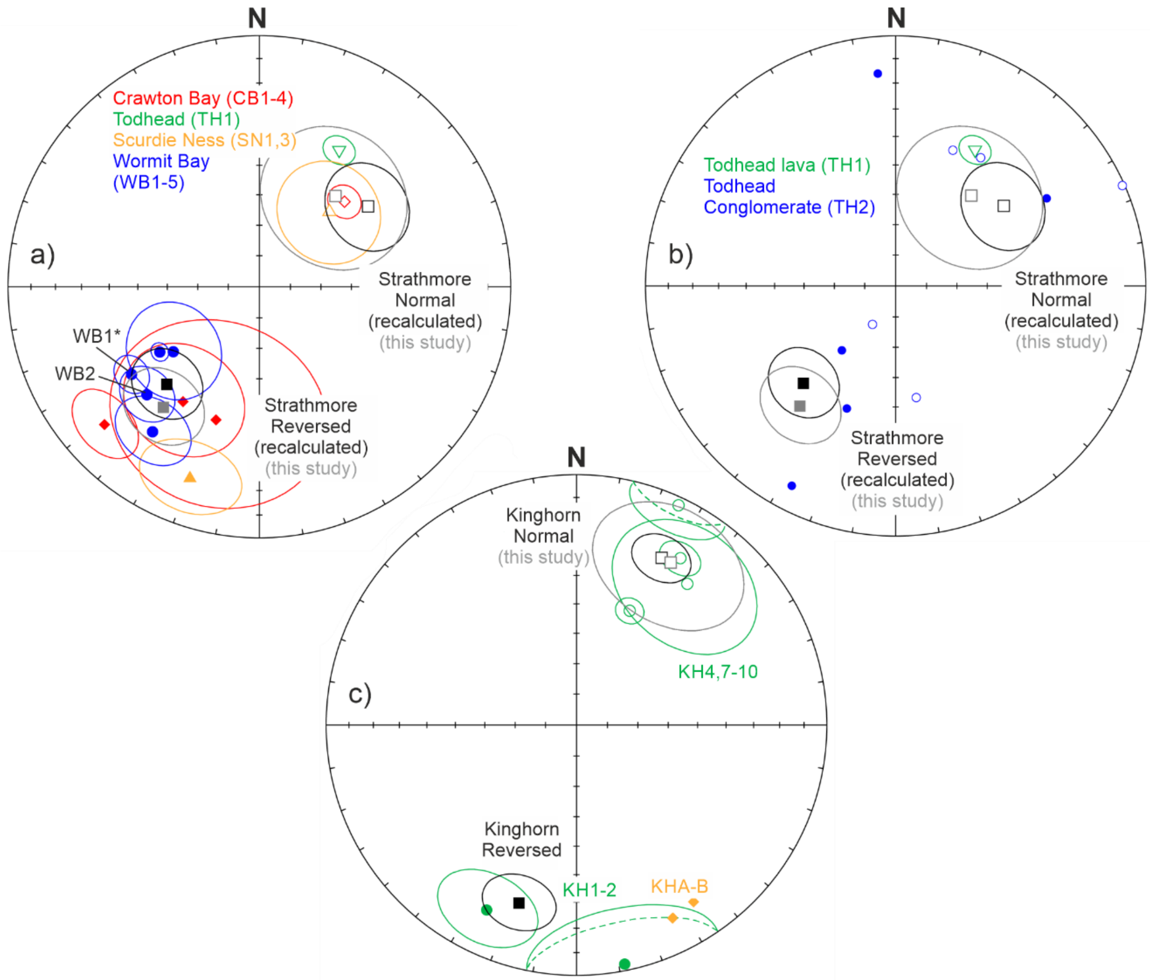

Fig. S2. Stereographic projections of (a) the accepted site mean directions from the Strathmore region, (b) the individual directions used for the conglomerate test for TH2 and (c) the accepted site mean directions from the Kinghorn lava flows. The site means are shown with their α_{95} circle. For the Strathmore site means (a), the new site directions from the different localities are represented by different colors and symbols; red diamonds (Crawton Bay), green inverted triangle (Todhead), orange triangles (Scurdie Ness) and blue circles (Wormit Bay). For the conglomerate test (b), the site mean for the TH1 lavas are as in (a) with blue circles for the individual conglomerate directions (TH2). For the Kinghorn sites (c), the new site directions are represented by green circles and the orange diamonds represent the average direction from the selected component from oriented paleointensity experiments for sites without separate paleointensity analysis (measurements from Grappone (65)). The black squares on both plots represent the locality mean directions used for the paleomagnetic poles from Torsvik (3) for Strathmore, recalculated to fit with modern paleodirectional analysis (see *Geological Background and Sampling; Strathmore Locality* for more details), and Torsvik et al. (20) for the Kinghorn. The gray squares are the recalculated normal and reverse directions from this study (the Kinghorn Reversed direction is not included as it is very poorly constrained due to a lack of sites).

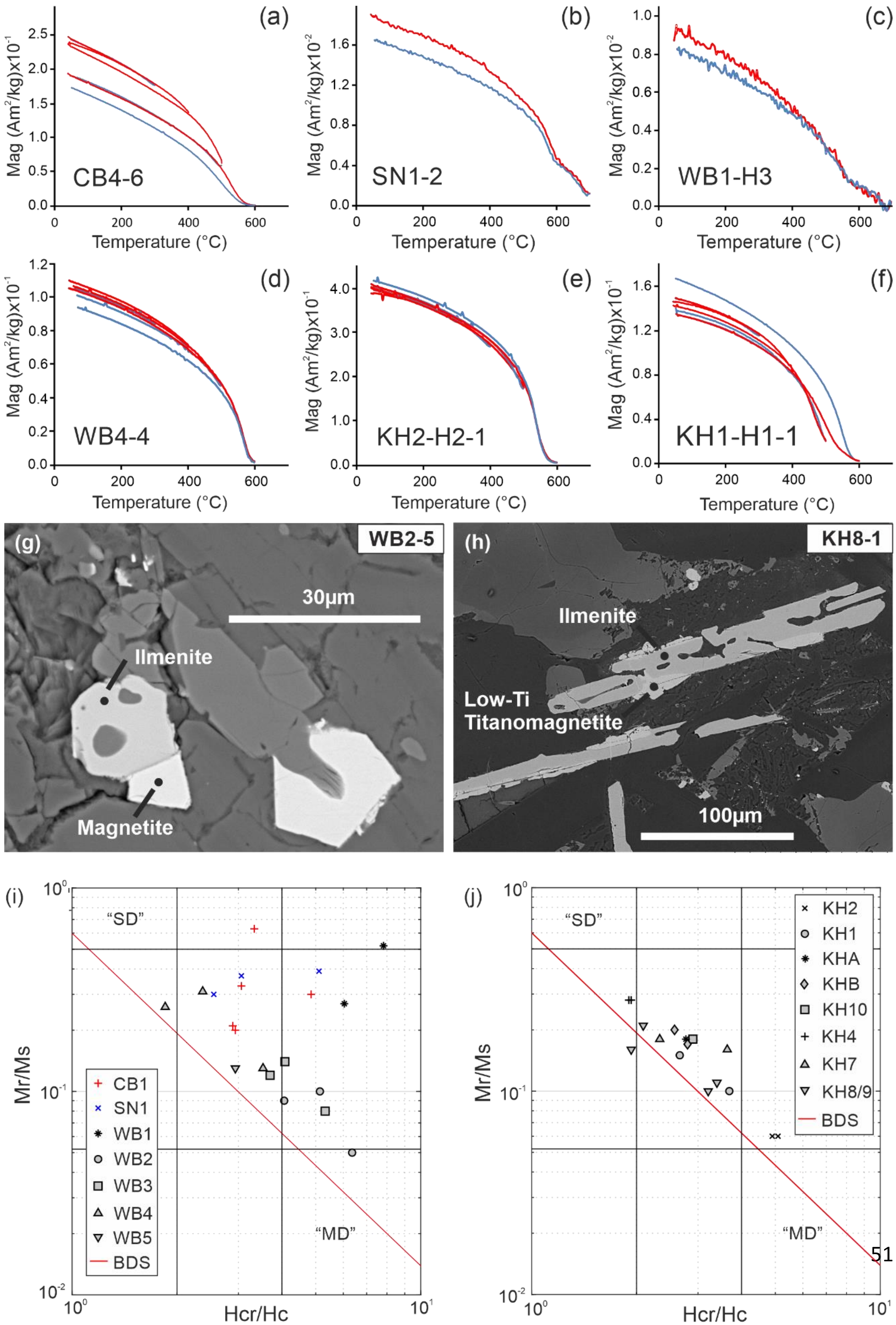

(a)
CB4-6
(b)
SN1-2
(c)
WB1-H3
(d)
WB4-4
(e)
KH2-H2-1
(f)
KH1-H1-1
Temperature (°C)
Mag (Am²/kg)x10⁻¹
Mag (Am²/kg)x10⁻²
(g)
WB2-5
30μm
Ilmenite
Magnetite
(h)
KH8-1
Ilmenite
Low-Ti Titanomagnetite
100μm
(i)
"SD"
"MD"
CB1
SN1
WB1
WB2
WB3
WB4
WB5
BDS
(j)
"SD"
"MD"
KH2
KH1
KHA
KHB
KH10
KH4
KH7
KH8/9
BDS
Mr/Ms
Hcr/Hc

Fig. S3. Representative thermomagnetic curves (a-f), representative BSE SEM images (g-h) and (i-j) hysteresis data plotted on an H_{cr}/H_c vs. M_r/M_s or “Day” plot from the sites that provided accepted paleointensity estimates. The thermomagnetic curves show the magnetization of the sample upon heating (red curve) and cooling (blue curve). The first four thermomagnetic curves (a-d), the left SEM image (g), and the left “Day” plot (i) are representative of the Strathmore sites while the rest are representative of the Kinghorn sites. The hematite bearing sites show thermomagnetic curves (b-c) with a single heating or cooling curve to 700 °C, while the other curves (a, d-f) were heated in steps of 100 °C, from 300-600 °C to show the temperature range over which the curves are (ir)reversible, indicating the presence of alteration. For the SEM images (g-h), the key magnetic minerals are labelled, having been identified from the EDX and igneous textures. The H_{cr}/H_c vs. M_r/M_s or “Day” plots (i-j) show the hysteresis data from all the samples that provided accepted paleointensity measurements; the red bulk domain state (BDS) line comes from Paterson et al. (34) and the black lines represent the grain size boundaries from Dunlop (66) with the “single-domain” (“SD”) and “multi-domain” (“MD”) boxes highlighted.

Table S1. Summary of the accepted site and locality mean directional data from the new Strathmore and Kinghorn sites, as well as the recalculated Strathmore sites from Torsvik (3).

Site	S_{LAT} (°)	S_{LONG} (°)	N (n)	D_G (°)	I_G (°)	D_S (°)	I_S (°)	k	α_{95}	P_{LAT}
Strathmore Locality:										
Crawton Bay										
CB1	56.9080	-2.2022	11	33.5	-62.3	45.0	-50.4	71.2	5.4	-43.6
CB2	56.9077	-2.2001	7	225.6	31.1	228.3	18.4	33.7	10.5	16.8
CB3	56.9081	-2.1980	4	202.2	54.2	213.6	44.1	24.5	18.9	34.8
CB4	56.9083	-2.1992	3	184.9	50.5	198.1	43.5	15.0	33.0	31.2
Todhead										
TH1	56.8848	-2.2161	10	22.6	-51.1	30.3	-37.2	99.7	4.9	-31.8
Scurdie Ness										
SN1	56.6910	-2.4424	10	44.1	-16.0	50.6	-64.6	25.5	9.8	-8.2
SN2	56.6952	-2.4415	4	16.6	-12.9	357.6	-55.7	2.1	88.0	-6.5
SN3	56.6810	-2.4507	8	199.0	-26.7	200.0	19.8	16.7	13.9	-14.1
Wormit Bay										
WB1	*56.4241*	*-2.9849*	*8*	*250.9*	*21.2*	*235.5*	*38.1*	*90.1*	*5.9*	*11.0*
WB2	56.4244	-2.9847	8	244.8	24.8	227.1	38.3	37.1	9.2	13.0
WB3	56.4237	-2.9857	8	230.8	22.3	215.8	29.1	24.5	11.4	11.6
WB4	56.4207	-2.9911	9	261.3	36.2	234.8	55.7	18.4	12.3	20.1
WB5	56.4207	-2.9911	8	261.2	31.2	239.5	51.5	143.3	4.6	16.8
New locality means										
Normal	-	-	3	-	-	40.0	-51.1	28.5	23.5	-31.7
Reverse	-	-	8	-	-	218.6	38.4	20.0	12.7	21.6
Combined	-	-	11	-	-	218.9	41.9	21.2	10.2	24.2
Redone Torsvik locality means										
Normal	-	-	6	-	-	53.5	-45.3	24.3	13.9	-26.8
Reverse	-	-	9	-	-	223.5	45.3	21.3	11.4	26.8
Combined	-	-	15	-	-	227.5	45.4	23.0	8.1	26.9
Kinghorn locality:										
Kinghorn sites										
KH2	56.0586	-3.2233	2	209.6	5.8	205.9	18.8	318.6	14.0	2.9

KH1	56.0625	-3.1793	2	169.7	3.2	168.6	2.8	118.7	23.1	1.6
KHA*	56.0621	-3.1782	1 (4)	166.2	-3.5	166.0	4.8	7.0	37.5	2.4
KHB*	56.0622	-3.1777	1 (2)	153.6	14.9	146.5	16.3	1412.3	6.7	8.3
KH10	56.0626	-3.1749	8	24.3	8.3	24.9	-3.7	21.9	12.1	-1.8
KH3	56.0633	-3.1739	3	32.3	6.8	32.3	-7.3	2.2	121.1	3.4
KH4	56.0639	-3.1734	8	38.9	-34.1	25.0	-48.3	162.2	4.4	-18.7
KH5	56.0643	-3.1733	4	257	50.4	253.6	76.3	1.5	128.2	31.1
KH6	56.0645	-3.1730	2	39.5	43.6	48.4	28.7	5	-	25.5
KH7	56.0669	-3.1735	7	36.2	-10.0	31.9	-22.6	103.4	6.0	-5.1
KH8/9	56.0680	-3.1738	11	43.3	-14.9	38.1	-29.1	49.6	6.5	-15.5
New locality means										
Normal	-	-	4	-	-	30.1	-26.0	18.0	22.3	-13.7
Reverse	-	-	2	-	-	186.7	11.4	8.4	102.1	5.7
Combined	-	-	6	-	-	22.0	-21.6	11.9	20.2	-11.2

S_{LAT} and S_{LONG}: site longitude and latitude; N (n): Number of samples (number of specimens); D_G and I_G: (anchored) Declination and Inclination in geographic co-ordinates; D_S and I_S: (anchored) Declination and Inclination in stratigraphic co-ordinates i.e. tectonically corrected; k and α_{95}: the precision parameter and 95% confidence limit from Fisher statistics (12); P_{LAT}: Paleolatitude. The sites that have been greyed out were not included in the new locality means. For the majority of sites, this was because the site mean directions were not clustered (k <15; k values with these values are underlined, as well as high α_{95} values >45°). *Sites with an asterisk next to them were not included in the locality means as the site directions came from the paleointensity measurements from a single hand sample (N=1*). WB1 was included for a baked contact test (passed) so it should have the same direction as WB2 and was, therefore, not included in the locality mean.*

Table S2. Statistics for the PRE, PCRS and POST bins and the results of Kolmogorov-Smirnov test for different levels of Q_{PI} filtering and age binning of the datasets.

Statistics		Q_{PI} ≥1	Q_{PI} ≥2	Q_{PI} ≥3	Q_{PI} ≥4	Q_{PI} ≥5	AGE+ ALT+ MD	Binned (Q_{PI} ≥1; 10Ma)	Binned (Q_{PI} ≥3; 10Ma)	Binned (Q_{PI} ≥1; 5Ma)	Binned (Q_{PI} ≥3; 5Ma)
		Q_{PI} filter									
Bin statistics:											
	N(*)	118	102	65	38	30	47	10*	9*	14*	12*
PRE bin statistics	***Age mean ± std.dev (skewness)***	378.0 ± 25.2 (-0.64)	376.7 ± 25.3 (-0.55)	371.3 ± 28.4 (-0.10)	376.4 ± 28.5 (-0.39)	374.5 ± 27.0 (-0.18)	361.8 ± 27.6 (0.56)	-	-	-	-
	VDM median/ IQR (V%)	18.4/ 26.1 (142 %)	17.5/ 25.8 (147 %)	17.0/ 26.8 (158 %)	14.1/ 10.7 (76%)	13.6/ 8.6 (63%)	15.7/ 13.2 (84%)	17.0/ 9.8 (58%)	17.9/ 30.1 (168 %)	16.5/ 7.0 (42%)	17.9/ 29.5 (165 %)
	N(*)	222	174	75	21	2	34	5*	4*	7*	6*
PCRS bin statistics	***Age mean ± std.dev (skewness)***	290.7 ± 10.6 (-0.14)	288.7 ± 10.4 (0.12)	283.1 ± 8.4 (0.63)	279.0 ± 6.7 (-0.16)	265.4	278.9 ± 5.3 (0.52)	-	-	-	-
	VDM median/ IQR (V%)	91.0/ 49.0 (54%)	94.0/ 55.0 (59%)	80.0/ 66.8 (84%)	48.0/ 42.3 (88%)	89.0/ 8.0 (9%)	45.5/ 41.0 (90%)	56.5/ 56.0 (99%)	79.8/ 62.5 (78%)	39.0/ 54.0 (138 %)	65.5/ 76.5 (117 %)
	N(*)	147	147	126	98	14	90	3*	2*	3*	3*
POST bin statistics	***Age mean ± std.dev (skewness)***	249.2 ± 11.0 (-4.02)	249.2 ± 11.0 (-4.02)	250.6 ± 7.8 (-6.14)	251.6 ± 5.2 (-9.73)	251.9 ± 0.3 (-1.26)	251.5 ± 5.4 (-9.31)	-	-	-	-
	VDM median/ IQR (V%)	24.6/ 15.5 (63%)	24.6/ 15.5 (63%)	23.6/ 14.5 (61%)	22.3/ 12.5 (56%)	23.6/ 19.0 (81%)	21.4/ 12.6 (59%)	35.3/ 35.5 (101 %)	26.7/ 6.7 (25%)	31.9/ 27.6 (87%)	28.6/ 10.0 (35%)

Kolmogorov-Smirnov tests:

p values	***PRE vs. PCRS***	1.3E-35	2.5E-29	1.4E-14	2.3E-06	2.2E-02	9.0E-07	2.2E-03	2.2E-02	6.0E-03	1.9E-01
	PCRS vs. POST	4.6E-45	2.5E-40	2.2E-23	1.2E-07	1.9E-02	1.4E-09	2.2E-01	4.7E-02	5.0E-01	2.0E-01
	PRE vs. POST	4.8E-04	3.5E-04	5.4E-04	9.7E-04	5.4E-02	1.8E-03	8.5E-02	4.0E-01	3.2E-02	4.4E-01
PRE vs. PCRS	***5%***	1	1	1	1	1	1	1	1	1	0
	1%	1	1	1	1	0	1	1	0	1	0
PCRS vs. POST	***5%***	1	1	1	1	1	1	0	1	0	0
	1%	1	1	1	1	0	1	0	0	0	0
PRE vs. POST	***5%***	1	1	1	1	0	1	0	0	1	0
	1%	1	1	1	1	0	1	0	0	0	0

Q_{PI}: the total Qualitive Paleointensity score based on the criteria defined by Biggin and Paterson (35); AGE/ALT/MD: three of the nine Q_{PI} criteria and sites must pass all three (each must score a 1) to be included in this dataset; PRE, PCRS and POST: primary age bins the VDM values from the updated PINT15 data (i.e. Dataset S3) were sorted into (from 315-416 Ma, 267-315 Ma and 200-267 Ma respectively); 10 Ma and 5 Ma, the 10 and 5 million year sub-bins the VDM values, were further divided into and the median values taken; N(*): the number of site mean estimates in the bin (*the number of sub-bins that included sites from the PINT15 database within that age range); std. dev.: standard deviation; VDM: virtual dipole moment; IQR: interquartile range; V%: IQR/median; p: asymptotic p-values from the Kolmogorov-Smirnov (k-s) test result; 5% and 1%: the significance levels the k-s tests were performed at; 1, 0 or NaN; pass, fail or insufficient data, in one or both of the bins, for the k-s test.

Dataset S1 (separate file). Summary of all the paleointensity results from the Strathmore locality. The selection criteria cut-offs applied to the paleointensity criteria are listed at the top; n: number of selected measurement steps; FRAC: fraction of the NRM used for the best fit of the selected component; β: scatter around the best fit of the selected component; q: 'quality factor'; $\left|\overrightarrow{k'}\right|$: curvature of the selected component; MAD_{ANC}: Maximum Angular Deviation (MAD) of the (anchored) best fit direction; α: angular difference between the best-fit anchored and free-floating directions; DRAT: maximum absolute difference from a pTRM check; CDRAT: cumulative DRAT. For further details on the selection criteria, the reader is referred to the Standard Paleointensity Definitions (SPD) (45). The two methods used for determining the paleointensity estimates were microwave (MW) and thermal with an AF cleanse (Th-AF) Thellier-type measurements using the IZZI protocol with pTRM checks. The maximum and minimum steps are shown as power integrals listed in Watt seconds (Ws) for the microwave measurements and temperature (T; °C) for the thermal experiments. Experimental results that do not pass the selection criteria are in gray, and the selection criteria that failed are underlined. Pi: Paleointensity estimate; H_{lab}: Applied lab field; s.d: Standard deviation.

Dataset S2 (separate file). Summary of all the paleointensity results from the Kinghorn locality. The selection criteria cut-offs applied to the paleointensity criteria are listed at the top; n: number of selected measurement steps; FRAC: fraction of the NRM used for the best fit of the selected component; β: scatter around the best fit of the selected component; q: 'quality factor'; $\left|\overrightarrow{k'}\right|$: curvature of the selected component; MAD_{ANC}: Maximum Angular Deviation (MAD) of the (anchored) best fit direction; α: angular difference between the best-fit anchored and free-floating directions; DRAT: maximum absolute difference from a pTRM check; CDRAT: cumulative DRAT. For further details on the selection criteria, see the Standard Paleointensity Definitions (SPD) (45). The two methods used for determining the paleointensity estimates were microwave (MW-IZZI) and thermal with an AF cleanse (Th-AF) Thellier-type measurements, using the IZZI protocol with pTRM checks. The maximum and minimum steps are shown as power integrals listed in Watt seconds (Ws) for the microwave measurements and temperature (T; °C) for the thermal experiments. Experimental results that do not pass the selection criteria are in gray, and the selection criteria that failed are underlined. Pi: Paleointensity estimate; H_{lab}: Applied lab field; s.d: Standard deviation.

Dataset S3 (separate file). All the PINT15 (67) data from between 200-500 Ma (under 'PINT data'), updated and scored for Q_{PI} ('Q_{PI} scoring'). All the headings under ‘PINT data’ are consistent with the headings from the PINT15 database and explained on the 'Information' sheet (available at http://earth.liv.ac.uk/pint/). Yellow cells represent those that have been updated/added since the last upload of the PINT15 database (excel comments on the top right cell of each block describe why the changes have been made). Sites that do not have a 'Data' number have either superseded previous sites (sites that have been superseded since the last PINT update are included at the bottom of the sheet in red) or have been added from studies published since the last update. The description for Dataset S4 gives the full refence for sites with a letter ref (a-e). The ‘Q_{PI} scoring’ headings are consistent with names of the nine different criteria, which are explained in detail in Biggin and Paterson (35), and the final Q_{PI} score ('Q_{PI}') is the sum of all the criteria (these are scored a 1 is they pass the criteria and 0 if they do not). The explanation for each of the site scores is given under the corresponding headings in Dataset S4.

Dataset S4 (separate file). Summary of the Q_{PI} scoring of all the sites from the updated PINT15 database (67) from between 200-500 Ma (i.e. Dataset S3). The ‘Study’ is given in the format of first author_publication year. The 'PINTref' number corresponds to the 'REF' in PINT15 (letters are for studies added in the Dataset S3 update) and ‘N’ is the number of sites included in the study. The abbreviations used in 'Method' are consistent with those on the 'PI Methods' sheet of the PINT15 database. The headings under 'Q_{PI} Values' are consistent with the nine Q_{PI} criteria which are explained in detail in Biggin and Paterson (35), and the final Q_{PI} score ('Q_{PI}') is the sum of all the criteria (these are scored a 1 is they pass the criteria and 0 if they do not). Cells with the same headings under 'Notes' provide explanations for the site scorings for the first eight criteria (MAG only passes only when the raw data is published, e.g. in the studies supplementary information, on the MagIC database, etc.). 'Other Notes' provides other information such as the revision of age dates based on newly published ages, how sites have been recalculated, why certain QPI criteria have been rescored since previously being published, etc. *a) Shcherbakova et al, 2015 (68), b) Anwar et al, 2016 (69), c) Shcherbakova et al, 2017 (31), d) Usui and Tian, 2017 (70) and e) Hawkins et al., 2019 (30).

SI References

1. M. Browne, R. Smith, A. M. Aitken, “Stratigraphical framework for the Devonian (Old Red Sandstone) rocks of Scotland south of a line from Fort William to Aberdeen” (2002).

2. N. H. Woodcock, “Early Devonian Sedimentary and Magmatic Interlude after Iapetus Closure” in *Geological History of Britain and Ireland*, Wiley Online Books., (2012), pp. 193–209.

3. T. H. Torsvik, Magnetic properties of the Lower Old Red Sandstone lavas in the Midland Valley, Scotland; palaeomagnetic and tectonic considerations. *Phys. Earth Planet. Inter.* 39, 194–207 (1985).

4. M. F. Thirlwall, Isotope geochemistry and origin of calc-alkaline lavas from a caledonian continental margin volcanic arc. *J. Volcanol. Geotherm. Res.* 18, 589–631 (1983).

5. M. F. Thirlwall, Geochronology of Late Caledonian magmatism in northern Britain. *J. Geol. Soc. London.* 145, 951–967 (1988).

6. J. B. Richardson, J. H. Ford, F. Parker, Miospores, correlation and age of some Scottish Lower Old Red Sandstone sediments from the Strathmore region (Fife and Angus). *J. Micropalaeontology* 3, 109–124 (1984).

7. J. T. Sallomy, J. D. A. Piper, Palaeomagnetic Studies in the British Caledonides - IV Lower Devonian Lavas of the Strathmore Region. *Geophys. Journal, R. Astron. Soc.* 34, 47–68 (1973).

8. T. H. Torsvik, *et al.*, Phanerozoic polar wander, palaeogeography and dynamics. *Earth-Science Rev.* 114, 325–368 (2012).

9. R. Van der Voo, The reliability of paleomagnetic data. *Tectonophysics* 184, 1–9 (1990).

10. M. R. Koymans, C. G. Langereis, D. Pastor-Galán, D. J. J. van Hinsbergen, Paleomagnetism.org: An online multi-platform open source environment for paleomagnetic data analysis. *Comput. Geosci.* 93, 127–137 (2016).

11. P. L. McFadden, M. W. McElhinny, Classification of the reversal test in palaeomagnetism. *Geophys. J. Int.* 103, 725–796 (1990).

12. L. Tauxe, R. F. Butler, R. Van der Voo, S. K. Banerjee, *Essentials of paleomagnetism.* (University of California Press, 2010).

13. M. Kono, N. Ueno, Paleointensity determination by a modified thellier method. *Phys. Earth Planet. Inter.* 13 (1977).

14. D. Stephenson, *et al.*, *Caledonian Igneous Rocks of Great Britain* (Joint Nature Conservation Commitee, 1999).

15. D. Stephenson, S. C. Loughlin, D. Millward, C. N. Waters, I. T. Williamson, *Carboniferous and Permian Igneous Rocks of Great Britain North of the Variscan Front* (Joint Nature Conservation Commitee, 2003).

16. A. Geikie, *The geology of central and western Fife and Kinross* (Mem. Geol. Surv. Scotland, 1900).

17. S. Brindley, E. Spinner, Palynological assemblages from Lower Carboniferous deposits, Burntisland district, Fife, Scotland. *Proc. Yorksh. Geol. Soc.* 47, 215–231 (1989).

18. A. A. Monaghan, M. A. E. Browne, "Nine 40Ar/39Ar dates from Carboniferous igneous rocks of the Midland Valley of Scotland" (2010).

19. F. J. Fitch, J. A. Miller, S. C. Williams, Isotopic ages of British Carboniferous rocks. *C.r. 6th Int. Congr. Carb. Strat. Geol. (Sheffield, 1967)* 2, 771–789 (1970).

20. T. H. Torsvik, O. Lyse, G. Atterás, B. J. Bluck, Palaeozoic palaeomagnetic results from Scotland and their bearing on the British apparent polar wander path. *Phys. Earth Planet. Inter.* 55, 93–105 (1989).

21. R. Van der Voo, The reliability of paleomagnetic data. *Tectonophysics* 184, 1–9 (1990).

22. J. L. Kirschvink, R. E. Kopp, T. D. Raub, C. T. Baumgartner, J. W. Holt, Rapid, precise, and high-sensitivity acquisition of paleomagnetic and rock-magnetic data: Development of a low-noise automatic sample changing system for superconducting rock magnetometers. *Geochemistry, Geophys. Geosystems* 9 (2008).

23. J. L. Kirschvink, The least-squares line and plane and the analysis of palaeomagnetic data. *Geophys. Journal, R. Astron. Soc.* 62, 699–718 (1980).

24. Y. Yu, L. Tauxe, Testing the IZZI protocol of geomagnetic field intensity determination. *Geochemistry, Geophys. Geosystems* 6 (2005).

25. R. S. Coe, S. Grommé, E. A. Mankinen, Geomagnetic paleointensities from radiocarbon-dated lava flows on Hawaii and the question of the Pacific nondipole low. *J. Geophys. Res.* 83, 1740–1756 (1978).

26. S. Levi, The effect of magnetite particle size on paleointensity determinations of the geomagnetic field. *Phys. Earth Planet. Inter.* 13, 245–259 (1977).

27. D. J. Dunlop, Ö. Özdemir, Beyond Néel's theories: Thermal demagnetization of narrow-band partial thermoremanent magnetizations. *Phys. Earth Planet. Inter.* 126, 43–57 (2001).

28. A. Biggin, M. Perrin, J. Shaw, A comparison of a quasi-perpendicular method of absolute palaeointensity determination with other thermal and microwave techniques. *Earth Planet. Sci. Lett.* 257, 564–581 (2007).

29. M. J. Hill, Y. Pan, C. J. Davies, An assessment of the reliability of palaeointensity results obtained from the Cretaceous aged Suhongtu section, Inner Mongolia, China. *Phys. Earth Planet. Inter.* 169, 76–88 (2008).

30. L. M. A. Hawkins, *et al.*, An exceptionally weak Devonian geomagnetic field recorded by the Viluy Traps, Siberia. *Earth Planet. Sci. Lett.* 506, 134–145 (2019).

31. V. V. Shcherbakova, *et al.*, Was the Devonian geomagnetic field dipolar or multipolar? Palaeointensity studies of Devonian igneous rocks from the Minusa Basin (Siberia) and the Kola Peninsula dykes, Russia. *Geophys. J. Int.* 209, 1265–1286 (2017).

32. G. A. Paterson, A. J. Biggin, E. Hodgson, M. J. Hill, Thellier-type paleointensity data from multidomain specimens. *Phys. Earth Planet. Inter.* 245, 117–133 (2015).

33. D. Heslop, A. P. Roberts, A Bayesian Approach to the Paleomagnetic Conglomerate Test. *J. Geophys. Res. Solid Earth* 123, 1132–1142 (2018).

34. G. A. Paterson, A. R. Muxworthy, Y. Yamamoto, Y. Pan, Bulk magnetic domain stability controls paleointensity fidelity. *Proc. Natl. Acad. Sci.* 114, 13120–13125 (2017).

35. A. J. Biggin, G. A. Paterson, A new set of qualitative reliability criteria to aid inferences on palaeomagnetic dipole moment variations through geological time. *Front. Earth Sci.* 2, 1–9 (2014).

36. G. A. Paterson, D. Heslop, A. R. Muxworthy, Deriving confidence in paleointensity estimates. *Geochemistry, Geophys. Geosystems* 11 (2010).

37. A. R. Muxworthy, M. E. Evans, S. J. Scourfield, J. G. King, Paleointensity results from the late-Archaean Modipe Gabbro of Botswana. *Geochemistry, Geophys. Geosystems* 14, 2198–2205 (2013).

38. L. Tauxe, T. Yamazaki, “Paleointensities” in *Treatise on Geophysics*, (2007), pp. 509–563.

39. J. Shaw, A New Method of Determining the Magnitude of the Palaeomagnetic Field: Application to five historic lavas and five archaeological samples. *Geophys. J. R. Astron. Soc.* 39, 133–141 (1974).

40. L. V de Groot, A. J. Biggin, M. J. Dekkers, C. G. Langereis, E. Herrero-Bervera, Rapid regional perturbations to the recent global geomagnetic decay revealed by a new Hawaiian record. *Nat. Commun.* 4, 2727 (2013).

41. E. Hodgson, J. M. Grappone, A. J. Biggin, M. J. Hill, M. J. Dekkers, Thermoremanent Behavior in Synthetic Samples Containing Natural Oxyexsolved Titanomagnetite. *Geochemistry, Geophys. Geosystems* 19, 1751–1766 (2018).

42. S. Xu, D. J. Dunlop, Thellier paleointensity theory and experiments for multidomain grains. *J. Geophys. Res. Solid Earth* 109 (2004).

43. P. Riisager, J. Riisager, Detecting multidomain magnetic grains in Thellier palaeointensity experiments. *Phys. Earth Planet. Inter.* 125 (2001).

44. G. A. Paterson, A simple test for the presence of multidomain behavior during paleointensity experiments. *J. Geophys. Res. Solid Earth* 116 (2011).

45. G. A. Paterson, L. Tauxe, A. J. Biggin, R. Shaar, L. C. Jonestrask, On improving the selection of Thellier-type paleointensity data. *Geochemistry, Geophys. Geosystems* 15, 1180–1192 (2014).

46. R. L. Wilson, The Thermal Demagnetization of Natural Magnetic Moments in Rocks. *Geophys. J. R. Astron. Soc.* 5 (1961).

47. R. L. Wilson, An Instrument for Measuring Vector Magnetization at High Temperatures. *Geophys. J. R. Astron. Soc.* 7 (1962).

48. R. Day, M. Fuller, V. A. Schmidt, Hysteresis properties of titanomagnetites: Grain-size and compositional dependence. *Phys. Earth Planet. Inter.* 13, 260–267 (1977).

49. A. J. Biggin, D. N. Thomas, The application of acceptance criteria to results of Thellier palaeointensity experiments performed on samples with pseudo-single-domain-like characteristics. *Phys. Earth Planet. Inter.* 138, 279–287 (2003).

50. P. A. Selkin, J. S. Gee, L. Tauxe, W. P. Meurer, A. J. Newell, The effect of remanence anisotropy on paleointensity estimates: A case study from the Archean Stillwater Complex. *Earth Planet. Sci. Lett.* 183, 403–416 (2000).

51. G. A. Paterson, The effects of anisotropic and non-linear thermoremanent magnetizations on Thellier-type paleointensity data. *Geophys. J. Int.* 193, 694–710 (2013).

52. A. Jackson, A. R. T. Jonkers, M. R. Walker, Four centuries of geomagnetic secular variation from historical records. *Philos. Trans. R. Soc. A Math. Phys. Eng. Sci.* 358, 957–990 (2000).

53. R. J. Veitch, I. G. Hedley, J.-J. Wagner, An investigation of the intensity of the geomagnetic field during roman times using magnetically anisotropic bricks and tiles. *Arch. Sci. Geneve.* 37, 359–373 (1984).

54. M. H. Dodson, E. McLelland-Brown, Magnetic blocking temperatures of single-domain grains during slow cooling. *J. Geophys. Res.* 85, 2625–2637 (1980).

55. S. L. Halgedahl, R. Day, M. Fuller, The effect of cooling rate on the intensity of weak-field TRM in single- domain magnetite. *J. Geophys. Res.* 85, 3690–3698 (1980).

56. F. D. Stacey, The physical theory of rock magnetism. *Adv. Phys.* 12, 45–133 (1963).

57. Y. Yu, Importance of cooling rate dependence of thermoremanence in paleointensity determination. *J. Geophys. Res. Solid Earth* 116 (2011).

58. A. J. Biggin, S. Badejo, A. R. Muxworthy, M. J. Dekkers, The effect of cooling rate on the intensity of thermoremanent magnetization (TRM) acquired by assemblages of pseudo-single domain, multidomain and interacting single-domain grains. *Geophys. J. Int.* 193, 1239–1249 (2013).

59. A. Ferk, *et al.*, Influence of cooling rate on thermoremanence of magnetite grains: Identifying the role of different magnetic domain states. *J. Geophys. Res. Solid Earth* 119, 1599–1606 (2014).

60. C. N. Santos, L. Tauxe, Investigating the Accuracy, Precision, and Cooling Rate Dependence of Laboratory-Acquired Thermal Remanences During Paleointensity Experiments. *Geochemistry, Geophys. Geosystems* 20, 383–397 (2019).

61. P. A. Selkin, J. S. Gee, L. Tauxe, Nonlinear thermoremanence acquisition and implications for paleointensity data. *Earth Planet. Sci. Lett.* 256, 81–89 (2007).

62. M. J. Hill, J. Shaw, Palaeointensity results for historic lavas from Mt Etna using microwave demagnetization/remagnetization in a modified Thellier-type experiment. *Geophys. J. Int.* 139, 583–590 (1999).

63. R. Shaar, L. Tauxe, Instability of thermoremanence and the problem of estimating the ancient geomagnetic field strength from non-single-domain recorders. *Proc. Natl. Acad. Sci. U. S. A.* 112, 11187–11192 (2015).

64. G. Kletetschka, P. J. Wasilewski, Grain size limit for SD hematite. *Phys. Earth Planet. Inter.* 129, 173–179 (2002).

65. J. M. Grappone, "Prototyping the next generation of versatile paleomagnetic laboratory," University of Liverpool. (2020).

66. D. J. Dunlop, Theory and application of the Day plot (Mrs/Ms versus Hcr/Hc) 1. Theoretical curves and tests using titanomagnetite data. *J. Geophys. Res. Solid Earth* 107 (2002).

67. A. J. Biggin, G. H. M. A. Strik, C. G. Langereis, The intensity of the geomagnetic field in the late-Archaean: New measurements and an analysis of the updated IAGA palaeointensity database. *Earth, Planets Sp.* 61, 9–22 (2009).

68. V. V. Shcherbakova, G. V. Zhidkov, V. P. Shcherbakov, A. V. Latyshev, A. M. Fetisova, Verifying the mesozoic dipole low hypothesis by the Siberian trap data. *Izv. Phys. Solid Earth* 51, 47–67 (2015).

69. T. Anwar, L. Hawkins, V. A. Kravchinsky, A. J. Biggin, V. E. Pavlov, Microwave paleointensities indicate a low paleomagnetic dipole moment at the Permo-Triassic boundary. *Phys. Earth Planet. Inter.* 260, 62–73 (2016).

70. Y. Usui, W. Tian, Paleomagnetic directional groups and paleointensity from the flood basalt in the Tarim large igneous province: Implications for eruption frequency. *Earth, Planets Sp.* 69 (2017).